

CHOLESTERYL HEMIAZELATE CAUSES LYSOSOME DYSFUNCTION IMPACTING VASCULAR SMOOTH MUSCLE CELLS HOMEOSTASIS

Liliana S. Alves¹, (liliana.alves@nms.unl.pt), André R. A. Marques^{1,*},
(andre.marques@nms.unl.pt), Nuno Padrão¹ (n.padiao@nki.nl), Filomena A.
Carvalho² (filomenacarvalho@medicina.ulisboa.pt), José Ramalho¹
(jose.ramalho@nms.unl.pt), Catarina Lopes²
(catarinalopes@medicina.ulisboa.pt), Maria I. L. Soares³ (misoares@ci.uc.pt),
Clare E. Futter⁴ (c.futter@ucl.ac.uk), Teresa M. V. D. Pinho e Melo³
(tmelo@ci.uc.pt), Nuno C. Santos² (nsantos@fm.ul.pt), Otilia V. Vieira^{1,*}
(otilia.vieira@nms.unl.pt)

1 Chronic Diseases Research Centre (CEDOC), NOVA Medical School, NOVA University Lisbon, 1169-056 Lisboa, Portugal.

2 Instituto de Medicina Molecular, Faculdade de Medicina, Universidade de Lisboa, Lisboa, Portugal.

3 CQC and Department of Chemistry, University of Coimbra, 3004-535 Coimbra, Portugal.

4 Department of Cell Biology, UCL Institute of Ophthalmology, London, U.K.

* Co-corresponding authors

Keywords:

Atherosclerosis; Oxidized lipids; Vascular smooth muscle cells; Lysosome dysfunction; Lysosome adaptation

Summary statement:

This article reports, for the first time, that a metabolite of cholesterol esters oxidation, found in plasma of cardiovascular disease patients, induces lysosome stress, culminating with the formation of vascular smooth muscle foam cells.

Abstract:

In atherosclerotic lesions, vascular smooth muscle cells (VSMCs) represent half of the foam cell population, characterized by an aberrant accumulation of undigested lipids within lysosomes. Loss of lysosome function impacts VSMCs homeostasis and disease progression. Understanding the molecular mechanisms underlying lysosome dysfunction in these cells is, therefore, crucial.

We identify cholesteryl hemiazelate (ChA), a stable oxidation end-product of cholesteryl-polyunsaturated fatty acid esters, as an inducer of lysosome malfunction in VSMCs. ChA-treated VSMCs acquire a foam cell-like phenotype, characterized by enlarged lysosomes full of ChA and neutral lipids. The lysosomes are perinuclear and exhibit degradative capacity and cargo exit defects. Lysosome luminal pH is also altered. Even though, the transcriptional response machinery and autophagy are not activated by ChA, the addition of recombinant lysosomal acid lipase (LAL) is able to rescue lysosome dysfunction. ChA significantly affects VSMCs proliferation and migration impacting atherosclerosis.

In sum, this work shows that: 1) ChA is sufficient to induce lysosomal dysfunction in VSMCs; 2) In ChA-treated VSMCs, neither lysosome biogenesis nor autophagy are triggered; and 3) Recombinant LAL can be a therapeutic approach for lysosomal dysfunction.

Introduction:

Vascular smooth muscle cells (VSMCs) play a crucial role in the development of cardiovascular diseases (CVDs). VSMCs have been implicated in all stages of human atherosclerotic plaque development. In early stages of the disease, VSMCs are responsible for the intimal thickening due to increased proliferation, migration and production of extracellular matrix (Newby & Zaltsman, 1999). This aberrant VSMC migration and proliferation culminates with the formation of a fibrous cap that is regarded as an adaptive response to atheroma formation and beneficial rather than detrimental to the pathology (Allahverdian et al., 2018; Greig et al., 2012). Nevertheless, the role of VSMCs in atherogenesis is not entirely beneficial. VSMCs within atherosclerotic lesions can also acquire a macrophage-like phenotype originating foam cells, undergo apoptosis and senescence (Feil et al., 2014; Shankman et al., 2015). Indeed, studies suggest that around 50% and 70% of foam cells, characterized by an aberrant lysosomal and cytosolic lipid accumulation, in human and murine lesions, respectively are VSMC-derived (Allahverdian et al., 2014; Vengrenyuk et al., 2015; Wang et al., 2019). The transformation of VSMCs into foam cells was first described in the 1970s, by de Duve, in the aorta of cholesterol-fed rabbits (de Duve, 1974). The sequestration of lipids, such as free cholesterol (FC) and cholesteryl esters, within lysosomes hinders their mobilization by cells, leading to lysosome dysfunction and enlargement (W. Gray Jerome & Lewis, 1990; Jerome et al., 1991; Minor et al., 1991). In VSMCs lysosome dysfunction may promote atherosclerosis by reducing their ability to clear dying cells and necrotic debris, exacerbating inflammation and promoting further cell death (Marques et al., 2021). Furthermore, lysosomes are the endpoint of the autophagic pathway, a critical process on VSMC function, phenotype, and survival (Xu et al., 2010; Ding et al., 2013).

In atherosclerotic lesions, the vast amount of oxidized low-density lipoproteins (oxLDL) generated in the arterial intima represents one of the sources of undigested lipids that accumulate within the lysosomes of foam cells (Yancey & Jerome, 1998). In VSMCs, oxLDL can be internalized by scavenger receptors and by micropinocytosis (Chellan et al., 2016). However, it remains unclear which components of oxLDL elicit the lysosomal dysfunction and subsequent

loss of VSMC homeostasis observed in atherosclerotic plaques. OxLDL represents a complex mixture of lipid oxidation products (Greig et al., 2012), making it difficult to associate a specific biological response with an individual oxLDL component and so, knowledge of the extent to which each oxidation product contributes to the pathology is required to further state any correlation between cause and effect.

Our group has identified and quantified cholesteryl hemiesters (ChE), stable oxidation end-products of cholesteryl-polyunsaturated fatty acid esters in LDL, in plasma of cardiovascular disease (CVD) patients and the most prevalent ChE is cholesteryl hemiazelate (ChA) (Estronca et al., 2012; Domingues et al., 2021, Matthiesen et al., 2021). In addition, as proof-of-concept, our group demonstrated that cholesteryl hemisuccinate (ChS), a commercially available but biologically irrelevant ChE, can induce irreversible lysosomal lipid accumulation and inflammation in macrophages, mimicking what has been described to occur in atherosclerotic lesions (Domingues et al., 2017; Estronca et al., 2012).

Considering the critical role of lysosomes in atherogenesis, it is imperative to extend our understanding of the molecular and cellular mechanisms underlying lysosomal dysfunction. For this reason, we decided to assess whether ChA can induce lysosomal dysfunction and loss of cell homeostasis in a murine model of VSMCs. Our data indicate that ChA is able to induce lysosome dysfunction in VSMCs leading to an exuberant accumulation of neutral lipids. The dysfunctional enlarged lysosomes are localized mainly in the perinuclear region of the cells and these outcomes can be the consequence of lysosomal luminal pH changes. Interestingly, the microphthalmia-transcription factor E (MIT/TFE) family of proteins, involved in responding and adapting to lysosomal stress, and autophagy are not activated. VSMCs with these features also proliferate and migrate less and become stiffer than control cells. Altogether, we present evidence that ChA is pathogenic towards VSMCs with potential impact in atherosclerosis progression and in their protective role in plaque stability.

Results:

ChA accumulates in enlarged perinuclear lysosomes in VSMCs

ChA is an amphiphile cholesterol derivative that acquires a negative charge at neutral pH (Fig. 1A). Given its poor solubility in cell culture medium, ChA was delivered to the VSMCs via ChA:POPC (1-palmitoyl-2-oleoyl-*sn*-glycero-3-phosphocholine) liposomes (65:35, molar ratio). POPC liposomes were always used as control. Based on our previous publications (Domingues et al., 2017; Domingues et al., 2021), we know that in macrophages ChE accumulate in late endosomal compartments (late endosomes/lysosomes, hereafter referred to as lysosomes). Similarly, to FC, ChE can be stained by filipin, a polyene macrolide antibiotic (Domingues et al., 2017, Domingues et al., 2021). Thus, we firstly analysed the intracellular distribution of ChA in VSMCs exposed to ChA:POPC liposomes. After 72 h incubation, we could observe a stronger and distinct filipin staining in cells treated with ChA:POPC, compared to POPC-exposed cells (Fig. 1B). In ChA-treated cells, filipin stained large round vesicular structures that were surrounded with the lysosomal-associated membrane protein 1 (LAMP1), a marker of lysosomes (Fig. 1B, insets). However, we cannot exclude that part of the filipin staining may be attributed to labelling of accumulated intralysosomal FC. Similar results were obtained when lysosomes were stained with LAMP2 antibodies. These data suggest that ChA causes the enlargement of lysosomes in VSMCs and that ChA may be accumulated inside these organelles. To better assess the impact of ChA in the lysosomal structure and the nature of the storage material, we performed a transmission electron microscopy analysis of VSMCs exposed to this lipid. Unlike control cells, VSMCs incubated with ChA liposomes revealed the presence of enlarged vesicular structures with electron-lucent material compatible with lipid accumulation visualized by light microscopy (Fig. 1C, red arrows). In accordance with previous observations (Domingues et al., 2017; Estronca et al., 2012), quantification of the area of lysosomes in VSMCs incubated with ChA for 72h showed a clear shift towards larger lysosomes compared to cells incubated with POPC liposomes (Fig. 1D). To confirm whether the observed enlargement was exclusive to lysosomes or impacted other organelles of the endocytic pathway, we immunostained VSMCs exposed to ChA for early-endosome

antigen 1 (EEA-1), a marker of early endosomes, and LAMP2. As shown in Fig. 1E, we did not see changes in the area of EEA-1 stained structures or colocalization of EEA-1 with LAMP2 in POPC or ChA-exposed VSMCs. Thus, indicating that the lipid-induced enlargement occurs exclusively in lysosomes and not in other organelles of the endocytic compartment.

Since it has been reported that cholesterol crystals can damage lysosome membranes with loss of its integrity, we decided to assess if ChA had a similar effect. For this purpose, we immunostained the ChA-treated VSMCs for Galectin-3 (Gal3), a protein that binds to sugars on the inner leaflet of lysosome membranes, which are exposed when lysosomes become permeable (Maejima et al., 2013). Thus, the presence of Gal3 on lysosomes indicates loss of lysosome membrane integrity. As shown in Fig. 1F, ChA-treated VSMCs lysosomes were not decorated with Gal3 punctae, indicating that the membrane of these organelles was kept intact. However, when ChA-treated VSMCs were challenged with an agent that permeabilizes lysosomal membranes acutely, the lysosomotropic di-peptide L-Leucyl-L-Leucine methyl ester (LLOMe), their lysosomal membranes were more sensitive to damage than lysosomal membranes of control VSMCs as judged by the presence of Gal3 punctae in lysosomes (Fig. 1F).

Exposure to ChA triggers neutral lipid accumulation and impairs acidification in VSMC lysosomes

Next, we sought to clarify the consequences of the detected enlargement and ChA accumulation for lysosomal homeostasis and function. Firstly, we investigated the storage of other lipids besides ChA/FC in the ChA-exposed lysosomes. Using the fluorescent neutral lipid dye BODIPY 493/503, we found that the LAMP2-positive enlarged lysosomes in VSMCs incubated with ChA were enriched in neutral lipids (Fig. 2A, see insets). In contrast, in POPC-exposed cells, there were no detectable BODIPY-positive lysosomes and just a limited number of small lipid droplets (Fig. 2A, see insets), indicating that neutral lipids are not being stored under these conditions. ChA, as stated above, is a polar lipid and cannot be visualized with BODIPY. However, we can speculate

that once ChA starts to accumulate in lysosomes the degradative capacity of these organelles is compromised, leading to the accumulation of internalized neutral lipids that exist in the cell culture medium, as well as other cargo, contributing to their enlargement. To assess if limited lysosomal lipid exit capacity was also contributing to the enlargement in ChA-treated cells, we measured the egress towards the Golgi of the glycosphingolipid lactosylceramide (LacCer) conjugated with BODIPY. LacCer can be taken up by endocytosis and upon exiting the lysosomes it is routed to the Golgi and not to the plasma membrane (Choudhury et al., 2002; Sharma et al., 2003). We evaluated the exit of LacCer from lysosomes in live cells by analysing the co-localization with the probe LysoTracker, which stains acidic organelles. ChA-treated VSMCs presented higher levels of LacCer co-localization with LysoTracker-positive vesicles (Fig. 2B, thick arrows) when compared with POPC-treated cells that show already some LacCer in the Golgi (Fig. 2B, thin arrows) which was quantified in Fig. 2C. These data suggest an impairment of lysosomal cargo exit due to ChA-treatment.

Then, we decided to evaluate the impact of ChA in lysosomal luminal pH. Breakdown of incoming endocytic and autophagic substrates within lysosomes, is pH dependent and, changes in pH could explain the outcomes described above (Fig. 2 A, B & C). The lysosomal pH gradient is assured by the activity of a proton-pumping V-type ATPase (Mindell, 2012). We probed lysosomal pH in VSMCs treated with ChA employing a combination of two dextrans, which readily reach lysosomes via the endocytic pathway: a pH insensitive dextran conjugated with Alexa 647 and a pH-sensitive dextran conjugated with fluorescein isothiocyanate (FITC). VSMCs exposed to ChA for 72h presented an approximately two-fold higher dextran-FITC/dextran-647 ratio, when compared to POPC-treated cells (Fig. 2D & E), indicating a significant increase in intralysosomal pH. Bafilomycin treatment was used as a positive control (Fig. 2E). Thus, lysosome luminal pH changes may be one of the mechanisms by which ChA causes the accumulation of undigested material within lysosomes.

Next, we determined the activity of several lysosomal hydrolases in ChA-treated VSMCs using artificial fluorescent substrates (in *ex vivo* assays). The activities of the glycosidases β -hexosaminidase and β -galactosidase were similar

between the lysates of POPC- and ChA-treated cells (72h incubation) (Fig. 2F). In contrast, the activity of the lysosomal acid lipase (LAL, encoded by the *Lipa* gene) as well as cathepsin B (CTSB) activity were about 30% decreased in ChA-treated VSMCs when compared to POPC-treated cells (Fig. 2F). Like cathepsins, LAL is synthesized as a zymogen, requiring proteolytic processing at low pH to become active (Ameis et al., 1994; Zschenker et al., 2004). On the other hand, cathepsin D (CTSD) activity was increased in ChA-exposed cells, which may be the consequence of the reported self-activation of pro-CTSD in the acidic assay buffer conditions. In general, these data indicate that in ChA-treated VSMCs the activity of lysosomal hydrolases is either unchanged (β -hexosaminidase and β -galactosidase) or decreased (CTSB and LAL).

To clarify if ChA was directly affecting the CTSB and LAL activity, we performed *in vitro* inhibition assays employing human recombinant enzymes in the presence of POPC or ChA liposomes. While increasing ChA concentrations did not significantly alter the activity of recombinant CTSD (data not shown), CTSL (data not shown) or LAL (Fig. 2G) towards their respective artificial substrates, CTSB activity towards the Z-Arg-Arg-AMC substrate was progressively inhibited (Fig. 2H). In this assay, CTSB activity was reduced by up to 20% of control levels in the presence of ChA liposomes (Fig. 2H), suggesting that this lipid may be able to directly inhibit the protease. To confirm whether CTSB inhibition by ChA plays a role in the cellular phenotypes observed, we decided to expose VSMCs simultaneously to ChA and a specific CTSB inhibitor, ZRLR (Reich et al., 2009; Wiczerzak et al., 2007). Indeed, pharmacological abrogation of CTSB activity led to a significant worsening of the lysosomal phenotype (Fig. 2I), as evaluated by the percentage of cells presenting enlarged lysosomes at 48h (Fig. 2J). Suggesting that CTSB inhibition may contribute to the development of the lysosomal phenotype observed. This led us to speculate whether boosting the activity of CTSB and LAL could prevent the accumulation of neutral lipids and consequent lysosomal enlargement. LAL is responsible for the breakdown of LDL-derived cholesteryl esters and triglycerides within lysosomes and recombinant enzyme is used as a treatment for patients suffering from LAL-deficiency. Following the same rationale, we decided to perform a rescue experiment in which VSMCs were treated with ChA liposomes

for 48h followed by a 24h exposure to recombinant human CTSB and/or LAL in the culture media. Treatment with rhLAL was able to fully revert the lysosomal hypertrophy (Fig. 2K and L) and neutral lipid accumulation (Fig. 2K) caused by ChA. The results with rhCTSB did not reveal a significant improvement under these experiment conditions, which may relate to the relatively long maturation time (> 24h) of rhCTSB taken up by endocytosis (di Spiezio et al., 2021).

As described for other experimental settings (Martina et al., 2016), lysosomal stress could trigger the activation of the MiT/TFE family of transcription factors (TF) with subsequent increase in lysosome biogenesis and autophagy (Napolitano & Ballabio, 2016). Therefore, next we decided to assess if ChA was promoting the nuclear translocation and activation of these TFs.

MiT/TFE transcription factors are not activated by ChA

The cellular localization and activity of MiT/TFE TFs is mainly controlled by their phosphorylation status. They are phosphorylated by the mechanistic target of rapamycin complex 1 (mTORC1) or other kinases, and localized in the cytosol in their inactive form (Settembre et al., 2013; Medina et al., 2015). Upon starvation or conditions of lysosomal dysfunction, TFs are quickly dephosphorylated and translocated to the nucleus, where they activate the transcription of the CLEAR gene network leading to an up-regulation of genes involved in lysosome functioning and autophagy (Martina et al., 2016; Napolitano & Ballabio, 2016). Taking this into account, we studied the translocation into the nucleus of TFEB, TFE3 and MiTF at different time-points in VSMCs treated with ChA or POPC. Torin-1 and Torin-2, inhibitors of mTOR activity, were used as positive controls. We found a significant increase in the nuclear fraction of MiTF 24 and 48h of ChA treatment, compared to POPC-treated cells (Fig. 3A-B) and an increase in nuclear TFE3 48h after treatment (Fig. 3C-D). Curiously, we did not observe nuclear translocation of TFEB in VSMCs stably expressing human TFEB-GFP (hTFEB-GFP, Fig. 3E-F). To assess whether this could have been an earlier event, we performed the same analysis at earlier time-points (Fig. S1A-F). At these time-points, there was also no significant increase in the nuclear fraction of hTFEB (Fig. S1E-F).

Importantly, at 72h of incubation, when changes at the lysosomal level were striking, ChA treated cells showed decreased levels of total hTFEB-GFP protein (Fig. 3G & H). Similar results were obtained for endogenous murine TFEB (Fig. 3G & I). Furthermore, increased levels of phosphorylated TFEB, its inactive form, were also observed (Fig. 3G & J).

Since mTOR is responsible for TFEB phosphorylation, we decided to address its activation status in ChA-treated VSMCs (Fig. 3K-M). The ratio phospho/total mTOR levels tend to be higher in ChA-treated than in control VSMCs (Fig. 3K and L). In addition, phospho-mTOR beautifully decorated the enlarged lysosomes in ChA-treated VSMCs (Fig. 3 M, insets). This led us to speculate that, at 72h ChA may be sufficient to hyperactivate mTOR, culminating with the phosphorylation of its effectors, namely TFEB.

Besides their nuclear translocation, the expression levels of these TFs have also been shown to increase upon exposure to lysosomal stressors (Lu et al., 2017; Pan et al., 2019). MiT/TFE family members are encoded by four distinct genes: *Mitf*, *Tfeb*, *Tfe3* and *Tfec* (Hemesath et al., 1994). To assess if ChA exposure might impact their transcription in VSMCs, we evaluated the expression level of these genes by qRT-PCR. VSMC starvation and treatment with Torin-1 were used as positive controls. No major alterations in the mRNA levels of the transcription factors *Mitf*, *Tfe3* and *Tfeb* were observed in ChA-treated, when compared to POPC-treated VSMCs (Fig. 4A-C). The only exceptions were a slight elevation in *Mitf* transcript levels after 24h incubation with ChA (Fig. 4A) and a decrease in *Tfe3* at 48 and 72h (Fig. 4B) and *Tfeb* expression at 24h (Fig. 4C).

Once in the nucleus, MiTF and TFE3 can promote cell adaptation to lysosome stress by upregulating transcription of numerous lysosomal and autophagic genes (Martina et al., 2016; Sergin et al., 2017). Thus, we assessed next the transcription levels of lysosomal genes (Fig. 4D-J) and autophagic genes (Fig. 4K-L) at different time-points. To our surprise, for all evaluated lysosomal and autophagic genes, we did not observe a significant transcription increase in ChA-treated VSMCs (Fig. 4D-L). In fact, the majority of the genes showed, at the later time-points, a reduction of their transcript levels when compared to POPC treated cells. We found that gene expression reduction was more

pronounced and significant for *Lipa*, *Mcln1*, *Lamp2b* and *Ctsb* (Fig. 4D, F, G and J) than for the other genes analysed. Interestingly, the decreased expression of the lysosomal genes coincided with the decline of lysosomal degradation capacity in ChA-treated cells (Fig. 2F).

Next, we analysed the protein levels of autophagy-related genes, whose transcription is decreased in ChA-treated cells (Fig. 4K-L). Microtubule-associated proteins 1A/1B light chain 3B (LC3) is an essential protein for autophagy, as it is crucial for substrate selection and autophagosome biogenesis. In particular, the levels of membrane associated (lipidated) LC3-II are commonly used as a marker for autophagosomes (Nakatogawa, 2020). At basal conditions, VSMCs treated with ChA presented a tendency towards higher levels of the lipidated LC3-II after 48h treatment with ChA liposomes, but this tendency was absent at 72h incubation (Fig. S2A and B). This suggests that the number of autophagosomes was not increased upon ChA-treatment and that autophagy was not stimulated. Another protein essential for autophagy is SQSTM1, an autophagy receptor that targets proteins for selective autophagy, which did not exhibit any change in our experimental settings (Fig. S2A and C). Since autophagy does not appear to be stimulated, this may indicate an impairment in autophagic cargo degradation due to lysosome dysfunction.

To gauge the autophagic flux in ChA-treated VSMCs, we inhibited the latter with the weak base chloroquine (CQ). CQ blocks the autophagic flux by increasing lysosomal pH, as well as decreasing autophagosome-lysosome fusion (Mauthe et al., 2018). As shown in Fig. S2B, the LC3-II/LC3-I ratio upon treatment with CQ in ChA-exposed and in control cells was similar. Overall, these data imply that, despite the translocation of MITF and TFE3, autophagy in murine VSMCs is not being stimulated by exposure to ChA. This outcome could be attributed, at least partially, to the mTOR activation and subsequent TFEB and possibly unc-51-like kinase (ULK) phosphorylation both autophagy inhibitors (Kim et al., 2011). Furthermore, the observation that lysosome membrane remains intact in ChA-treated cells (Fig. 1F) makes the occurrence of lysophagy unlikely.

In ChA-treated VSMCs the increase in lysosomal mass is not caused by an increase in lysosomal number

As we observed an inhibition of the transcription of lysosomal genes and, lysosomes of VSMCs are dysfunctional following exposure to ChA, we set out to investigate whether ChA exposure results in any change of structural and luminal lysosomal proteins. The protein levels of the lysosomal transmembrane protein LAMP1 were significantly increased in cells treated with ChA, in comparison to POPC-treated cells (Fig. 5A & B). Next, we evaluated the protein levels of luminal lysosomal cathepsins, some of the most abundant soluble lysosomal hydrolases. Analysis of CTSD protein levels revealed a significant increase in pro-CTSD levels (reflected in the total protein levels), which was not accompanied by an increase in mature (lysosomal) CTSD (Fig. 5C-E), suggesting that pro-CTSD is not being properly processed in the lysosomes to the mature (active) form of the enzyme (Marques et al., 2019). When CTSB protein levels were analysed an increase in its pro-form was also observed (Fig. 5F & G). Immunostaining of CTSD revealed an increase in protein levels within the enlarged lysosomes of ChA-exposed VSMCs (Fig. 5H-I). To understand whether the observed increase in LAMP1 and pro-cathepsins levels was complemented by a similar elevation in lysosome number, we counted the number of lysosomes in POPC- and ChA-treated VSMCs (72h incubation). Surprisingly, the number of lysosomes was significantly reduced in VSMCs exposed to ChA liposomes (Fig. 5J). Together, our observations indicate that even though lysosomal mass is increased, that did not translate into an increased number of lysosomes, but rather in the enlargement of these organelles. To further understand the increase in lysosomal mass we decided to evaluate if ChA was affecting lysosomal protein degradation. For that, we treated VSMCs with the translational inhibitor, cycloheximide, and after 6 and 12h post-chasing the total-CTSD levels were analysed. The relative levels of the protease (compared to t=0) were always higher in ChA-treated VSMCs than in control cells (Fig. 5K & L).

ChA affects VSMC proliferation

Next, we decided to evaluate the impact of lysosome dysfunction in VSMCs viability, an event that can contribute to plaque instability (M. O. Grootaert et al., 2015; M. O. J. Grootaert et al., 2018). We evaluated necrosis and apoptosis by Propidium Iodide (PI)/annexin V staining. Necrosis was also evaluated by lactate dehydrogenase (LDH) release at 72h incubation time. We found that ChA-treated cells did not present any increase in the staining by annexin V up to 72h, when compared with control cells (Fig. 6A). Moreover, when PI staining and LDH activity in the medium was measured, no differences between control and ChA-treated cells were observed (Fig. 6B). These results indicate that ChA treatment did not induce apoptosis or necrosis. However, observations under the microscope, suggested that in the presence of ChA the number of VSMC was lower in comparison with control cells. To confirm this observation, we counted the number of cells at 48 and 72h and, as shown in Fig. 6C, a significant decrease on cell number was observed at both time points in the presence of ChA (Fig. 6C). This can be achieved through delaying the proliferation rate and/or by arresting the cell cycle. To address these two hypotheses, we first evaluated Ki-67 mRNA levels. The results showed a significant decrease in *Ki-67* mRNA levels at 72h, under ChA conditions (Fig. 6D). Given these results, we further evaluated the proliferation using the vital dye CarboxyFluorescein Succinimidyl Ester (CFSE), whose fluorescence intensity decreases with every cell division. As expected, CFSE fluorescence intensities in ChA-treated VSMCs at 48 and 72h were higher than for the controls (Fig. 6E). These results suggest that there is a decline in VSMCs proliferation. Taking these results into account, together with the increase in lysosomal mass, we decided to search for cell senescence markers in VSMCs exposed to ChA.

Cellular senescence can be established by the activation of two different tumor suppressor pathways: CDKN2A(p16)-RB (retinoblastoma) and TP53-cyclin-dependent kinase inhibitor1A (CDKN1A, p21). Thus, we assessed whether these two senescent pathways were activated in VSMCs treated with ChA. As shown in Fig. 7A & B, at 48h p16 levels were higher in ChA-treated than in control cells. This is in line with the lower number of cells at 48 h (Fig. 6C).

Nevertheless, p16 levels at 72h returned to POPC expression levels. Yet, when we evaluated p21 protein levels, we could observe an increase in ChA-treated cells compared to controls at 72h (Fig. 7C-D). The expression of p21 is orchestrated by the transcription factor p53, which promptly translocates to the nucleus in response to different stress signals driving p21 expression. After 72h exposure to ChA, VSMCs presented a significantly increased ratio of nuclear vs. cytoplasmic p53, evidencing its nuclear translocation (Fig. 7E & F). This is in line with the increased p21 expression levels at this time point. However, this outcome did not result in γ H2AX, a histone involved in DNA repair, translocation into the nucleus (Fig. 7G), suggesting that our results are more compatible with a state of reversible cell cycle arrest (quiescence) than with cell senescence. Similarly, ChA-treated VSMCs do not exhibit a senescence-associated secretory phenotype (SASP) as shown in Fig. 7H-K.

VSMC migration and elasticity are decreased upon ChA treatment

VSMC migration to the intima is one of the first steps of atherosclerosis, being critical to the formation of the protective fibrous cap over the atheroma. Lysosomal dysfunction may influence VSMC migration, as traffic of some migration machinery goes through the late endosome/lysosome/plasma membrane pathway, namely integrins and matrix metalloproteinases (Dozynkiewicz et al., 2012; Monteiro et al., 2013). Thus, we investigated if ChA is able to alter the migration ability of VSMCs. These experiments were performed by wound healing in the presence of mitomycin C, to synchronize the cell cycle and ensure that the experiment was performed with a similar number of cells. The results revealed that VSMC migration was markedly reduced even at 4h post ChA-addition (Fig. 8A). Taking this into account, the decrease in VSMCs migration observed upon ChA-exposure may be associated with alterations in lysosome function, as some cells featured enlarged lysosomes already at 8h of ChA exposure (Fig. 8B, see insets). Afterwards, we evaluated the transmigration capacity of VSMCs after 72h of ChA exposure. The results indicated that the migration capacity of ChA-treated cells was decreased when compared to controls (Fig. 8C & D). Furthermore, taking the previous results into account, we hypothesized that the described lysosomal dysfunction of ChA-

treated cells may have a role in VSMC migration and trans-migration. To investigate this, we treated cells with CQ for 4h and measured their transmigratory pattern. The results revealed that upon CQ treatment, the migration capacity was strikingly reduced when compared with ChA treated and control cells (Fig. 8C & D). Overall, these results indicate that ChA treatment leads to a decrease in the migration capacity of VSMCs upon acute (8h) and chronic (72h) exposures, and that lysosomes may play an important role in this process.

ChA may also affect the biomechanical characteristics of cells, with consequences in migration and transmigration. To evaluate if ChA is altering the biomechanical properties of VSMCs, atomic force microscopy (AFM) measurements were performed. The AFM tip penetration depth and the Young's modulus were the quantitative parameters extracted from the AFM quantitative images, combining imaging with force spectroscopy. The results revealed that ChA treated cells present lower penetration depth, indicating that they are less capable to deform than control cells (Fig. 8E & F). Moreover, ChA-treated VSMCs showed a higher Young's modulus, when compared to the controls (Fig. 8E & G), also indicating that these cells are stiffer than their controls. Due to the force applied on the cells, the penetration depth values exceeded the thickness of cortical actin. Thus, it is expectable that lysosomes would also contribute to the observed increase in cell stiffness. From Fig. 8E (height images), it can also be noticed that VSMCs treated with ChA change their morphology, becoming less elongated and organized in a monolayer, when compared with the control cells. ChA-treatment lead to local changes on cell deformation (lower penetration depth), apparently at the cytoplasm level, when compared with the penetration depth QI image of the control cells.

Altogether, our data suggests that lysosome dysfunction, cell cycle arrest and changes of the biomechanical properties in ChA-treated VSMCs can lead to pro-atherogenic like phenotypes.

Discussion:

One of the early characteristics of atherogenesis, observed in lesions of different origin, is the sequestration of lipids by macrophages and VSMCs in their lysosomes. It is accepted that lysosome dysfunction is at the centre of the atherosclerosis pathogenic hub (Fowler, 1980; Fowler et al., 1980; Geer et al., 1961; W G Jerome & Lewis, 1985; Shio et al., 1979; Wolinsky et al., 1974; Yancey & Jerome, 1998). The decline in lysosomal function is postulated to cause and/or facilitate atherosclerosis. In contrast with the vast amount of literature on lysosome dysfunction in macrophages, very little is known about lysosome dysfunction in VSMCs. Here we found that ChA, a stable end oxidation product of cholesteryl linoleate and arachidonate found increased in plasma of CVD patients (Domingues et al., 2021; Matthiesen et al., 2021) accumulates in VSMCs and causes lysosome malfunction, recapitulating many of the effects seen with oxLDL, including induction of foam cell formation. We also demonstrate that, as consequence of these alterations, these cells become stiffer, migrating and proliferating less. Regarding the ChA concentrations employed, one should bear in mind that liposomes are not very efficient vehicles for ChA delivery (less than 3% of ChA is internalized) (Domingues et al., 2021), and so we expect the “real” ChA concentrations to be on the micromolar range. This corresponds to the range of concentrations found in the plasma of CVD patients (Domingues et al., 2021; Matthiesen et al., 2021).

ChA accumulates in lysosomes inhibiting cargo degradation and egress, culminating with lysosomal neutral lipid accumulation and acquisition of a foam-cell like phenotype. The dysfunctional lysosomes are enlarged and perinuclear. Furthermore, ChA-treated VSMCs exhibit an increase in lysosomal mass but have less lipid-loaded lysosomes than control VSMCs. These outcomes can be explained by the fact that ChA is an amphiphilic molecule and partitions via passive diffusion and trans-membrane translocation into all cell membranes. Thus, like cholesterol, it is expected that ChA affects membrane lateral packing density, causing changes in the v-ATPase activity, increased luminal pH and decreased acidic hydrolase activity (Maxson & Grinstein, 2014). It is also conceivable that lysosome dysfunction is not only caused by changes in the biophysical properties of cell membranes and lysosome pH. For example, it is

possible that ChA, like oxLDL, partly inactivates some lysosomal enzymes. Indeed, here we demonstrate that ChA can directly inhibit the activity of lysosomal CTSB. ChA is not a CTSB substrate, however we can envision that some hydrophobic interactions may occur between the lipid and the enzyme resulting in the inhibition of the latter. In line with this hypothesis, complete pharmacological inhibition of CTSB activity led to a worsening of the lysosomal phenotype in VSMCs exposed to ChA. In contrast, ChA does not appear to affect LAL activity *in vitro*. Nonetheless, the addition of recombinant LAL to ChA-treated VSMCs is sufficient to overcome lysosome enlargement and neutral lipid accumulation. As reported in the literature, these results can be explained by the low levels of LAL in VSMCs (Dubland et al., 2021). In our experimental set-up, the cells were exposed to ChA for 48h followed by a 24h treatment with rhLAL (in the absence of ChA). At the 48h timepoint, the changes in lysosomal pH are likely not as dramatic as observed at 72h, and in this way the processing of the exogenous LAL is not hindered by the alkalinization of the lysosomal pH, as described by Dubland et al., 2021. Thus, the addition of this recombinant enzyme will facilitate the hydrolysis of neutral lipids, with the loss of foam-cell phenotype.

An increase in lysosome area can then be explained by the accumulation of undigested material inside lysosomes or by the increase in lysosome fusion and decrease in fission or even by an increase in *de novo* lysosome biogenesis (de Araujo et al., 2020; Saffi & Botelho, 2019). However, in ChA-treated VSMCs the increase in lysosome area cannot be attributed to lysosomal biogenesis. As such, MiT/TFE transcription factors, key players in cellular adaptation to lysosome dysfunction, are not activated in ChA-treated VSMCs. TFEB nuclear translocation is even inhibited. The increase in lysosomal area and mass can also be driven by a delay in intracellular degradation of lysosomal protein components, similarly to what was described for LAMP2 in the absence of protein/cathepsin A (Cuervo et al., 2003). Another possibility is that mTOR mediates a TFEB-independent boost in lysosomal protein translation, similar to that shown to take place in macrophages (Hipolito et al., 2019). In order for this to occur, both S6K and 4E-BP effectors must be phosphorylated by mTORC1 (Hipolito et al., 2019). However, in our experimental settings, we could only

observe an increase in the phosphorylation of S6K but not 4E-BP (data not shown), making this hypothesis less likely.

ChA-treated VSMCs are also stiffer than control cells (Fig. S3, working model). The increase in cell stiffness may explain, in part, the effects on cell quiescence and migration that are crucial to form the fibrous cap that stabilizes atherosclerotic lesions. Finally, the increase in cell stiffness together with lysosome dysfunction could abrogate phagocytosis of lipids, dead cells and cell debris (Santarino et al., 2017; Viegas et al., 2012) contributing to the etiology and development of the atherosclerotic lesions.

Materials and methods

Cholesteryl hemiazelate (ChA, cholesteryl O-(8-carboxyoctanoyl)) synthesis

Cholesteryl hemiazelate (ChA, cholesteryl O-(8-carboxyoctanoyl)) was prepared following a general procedure described in the literature for the synthesis of cholesteryl hemisuccinate (Klein et al., 1974). However, in order to optimize reaction conditions, molar equivalents of the reactants, reaction time and purification conditions were adapted. The synthetic strategy involves the reaction of commercially available cholesterol with azelaic anhydride, which was prepared by the reaction of azelaic acid with acetyl chloride, as described elsewhere (Hill & Carothers, 1933). Cholesterol was reacted with 2.6 molar equivalents of azelaic anhydride in dry pyridine under reflux for 7 h. Purification by flash chromatography with chloroform/methanol/ammonia (50:5:0.25), followed by recrystallization from ethanol, gave the target cholesteryl hemiazelate as a white solid in 57 % yield. After the reaction, ChA is purified by flash chromatography with chloroform / methanol / ammonia (to remove unreacted cholesterol) and recrystallized from ethanol. ChA purity is assessed by NMR (^1H and ^{13}C) and melting point to ensure that the product is not contaminated with unreacted reagents, pyridine or any solvent.

Preparation of liposomes

Lipid aqueous suspensions were prepared by mixing POPC (Avanti Polar Lipids, Alabaster, AL, USA) and ChA at 35:65 molar ratio in an azeotropic mixture of chloroform and methanol, and then incubated for 30 min. The solvent was evaporated using a rotary evaporator and dried during 30 min in a 65°C water bath. The lipid film was hydrated with a buffer solution 20 mM Hepes, 0.11 M NaCl, 1 mM EDTA, pH 7.4 in a water bath at 65°C for at least 1 h. Samples were submitted to mild sonication for 10 min and extruded through a polycarbonate filters (Nucleopore, Whatman, Little Chalfont, UK) with a pore diameter of 0.4 µm. This process was repeated at least 6 times. During extrusion, the water-jacketed extruder (Lipex Biomembranes, Vancouver, British Columbia, Canada) was maintained at 65°C. ChA concentration was determined using the Liebermann-Burchard protocol (Huang et al., 1961).

Cell culture

Murine aorta smooth muscle cells (MOVAS, CRL-2797™, ATCC, Manassas, VA, USA) were grown in Dulbecco modified Eagle medium (DMEM GlutaMAX, Gibco, Thermo Fisher, Waltham, MA, USA) supplemented with 10% heat inactivated fetal bovine serum (FBS, Gibco), 1 mM pyruvate (Gibco) and 0.2 mg/mL G-418 (Sigma), and passaged 2 to 3 times before their use in the different assays. Cells were grown in a humidified incubator at 37°C under 5% CO₂. After 24 h of seeding, VSMCs were incubated with ChA:POPC (65:35, molar ratio, ChA) or POPC liposomes, as control, for up to 72 h, as indicated in the figure legends. The concentrations used in most of the experiments was 1500 µM ChA and 807.7 µM POPC (the equivalent to the POPC concentration present in ChA liposomes). The MOVAS cell line was recently authenticated and tested negative for mycoplasma contamination.

Stainings, imaging acquisition and analysis

Primary antibodies: anti-LAMP1 and anti-LAMP2 (1:500; Hybridoma Bank, 1D4B and ABL-93), anti-EEA-1 (1:50; Santa Cruz, SC-6415), anti-CTSD (1:100; SICGEN, AB0043-200), anti-MITF (1:50; Tebu-bio, B0512), anti-TFE3 (1:100; Sigma HPA023881), anti-p53 (1:50; SICGEN, AB0154-200), anti-SQSTM1 (1:50; Abgent, AP2183B); anti-Phospho-Histone H2A.X (1:500; Cell Signaling Technology, 20E3 #9718).

For immunofluorescence (IF) stainings, VSMCs were grown in the presence of lipids on glass coverslips. After incubation, cells were fixed with 4% paraformaldehyde (PFA) for at least 30 min, followed by quenching of the aldehyde groups with ammonium chloride and permeabilization with saponin (0.1 % in PBS). After permeabilization, cells were blocked with 1% BSA in PBS or for lipid staining 2% fish gelatin in PBS (Bodipy and filipin). Cells were then incubated with the primary antibodies in blocking solution for 1 h at room temperature (RT) (LAMP1 and 2, p53, SQSTM1, EEA-1, CTSD and H2A.X) or overnight (ON) at 4°C (MITF, TFE3 and TFEB). Then they were washed, and finally incubated for 1 h with the secondary antibodies conjugated with a fluorophore. Antibody dilution was 1:500 for secondary antibodies conjugated with Cy3 and 1:250 for those conjugated with Cy5. Secondary antibodies used were from Jackson ImmunoResearch Laboratories (West Grove, PA, USA). Neutral lipids were stained with Bodipy 493/503 (diluted 1:500 from a saturated ethanolic solution of Bodipy) for 1 h. Free cholesterol and ChA were stained with filipin (25 µg/mL in PBS) for 30 min at room temperature. DAPI was used to visualize nuclei (1:800; Fluka). Coverslips were mounted with mowiol/DABCO and images were obtained using an AxioVision microscope (Axio Observer Z2), a Zeiss LSM710 confocal microscope or a Zeiss LSM980 confocal microscope with a 63x oil-immersion objective, using the appropriate filter sets (1.4 NA).

Images were randomly acquired, and 10 different fields were imaged for each experimental condition. For a given staining, images were acquired with the same settings. Images were obtained from three independent experiments and in total more than 15 cells were analysed per condition. Quantification of the number and size of lysosomes was performed using ImageJ software.

Background was subtracted from the total fluorescence intensity of each region of interest (ROI). For nucleus translocation, the ratio of the nucleus and cytoplasm fluorescence intensities was calculated also using ImageJ.

Transmission electron microscopy

For transmission electron microscopy, cells were seeded on glass coverslips and, after POPC and ChA treatment, fixed in 2% PFA / 2% glutaraldehyde (Electron Microscopy Sciences, Hatfield, PA, USA) in 0.1 M phosphate buffer. Cells were then osmicated, treated with tannic acid, dehydrated, infiltrated with Epon and mounted on Epon stubs, all as previously described (Tomas et al., 2004). After polymerization overnight at 60°C, coverslips were removed from Epon stubs with liquid nitrogen. 70 nm sections were cut en face and stained with lead citrate, before examination on a Jeol 1010 transmission electron microscope and images acquired with a Gatan OriusSC100B charged couple device camera.

Lysosome pH measurement

Cells were seeded in a Nunc™ Lab-Tek™ Chamber Slide (Thermo Fisher) and treated for 3 days with ChA or POPC. At day 2, cells were incubated ON simultaneously with dextran conjugated with fluorescein-isothiocyanate – FITC-dextran (200 µg/mL; Sigma) and dextran conjugated with Alexa Fluor 647 (50 µg/mL; Thermo Fisher). To ensure that lysosomes were labelled by the ON pulse, cells were washed with fresh culture medium and analysed by fluorescence microscopy after 3h in dextran-free medium. Image acquisition was performed in CO₂-independent medium, and the settings were not changed between different samples. To measure the fluorescence intensity ratio between FITC-dextran and Alexa Fluor 647 within the lysosomes, the organelles were delimited and the fluorescence intensities of the two channels were quantified with ImageJ Fiji software (Coloc2 plugin).

Lactosylceramide egress

Cells were seeded in a Nunc™ Lab-Tek™ Chamber Slide (Thermo Fisher) and treated for 3 days with ChA or POPC. At day 3, cells were incubated with BODIPY® FL C5-Lactosylceramide – LacCer (2.5 μM; Invitrogen, Carlsbad, CA, USA) in DMEM with 1% FBS for 45 min and LysoTracker™ Red DND-99 (200 nM; Invitrogen) to stain the acidic organelles, for 15 min, at 37°C. Cell surface fluorescence of LacCer was removed by washing the cells 3 times with 10% serum. Cells were followed under a confocal microscope for 3 h at 37°C in DMEM with 10 mM Hepes and 10% FBS. Images were obtained for both dyes. Colocalization was calculated using the Manders (M1) coefficient from ImageJ JACoP plugin.

Lysosomal hydrolase activity

CTSD activity was assayed as previously described (Marques et al., 2019). CTSB activity was determined in a similar manner using 20 μM of cathepsin B substrate Z-RR-AMC (Enzo Life Sciences, Farmingdale, NY, USA) (di Spiezio et al., 2021) β-hexosaminidase activity was measured with 1.97 mM 4-methylumbelliferyl-N-acetyl-β-D-glucosaminide (Sigma) in 150 mM citrate-Na₂HPO₄ (pH 4.0) buffer. β-galactosidase activity was measured with 0.64 mM 4-methylumbelliferyl-β-D-galactoside (Sigma) in 150 mM citrate-Na₂HPO₄ (pH 4.0) buffer with 0.2 M NaCl. The 4-methylumbelliferyl (4-MU) substrates for these two glycosidases were kindly gifted by Prof. Johannes Aerts (University of Leiden, The Netherlands). For these two activities, after incubation at 37 °C for 30 min, the reaction was quenched with 0.3 M glycine adjusted with NaOH to pH 10.6. LAL activity was assayed based on the method described by (Hamilton et al., 2012), with slight alterations. Briefly, cells were lysed in reaction buffer (100 mM sodium acetate pH 4.0 with 1% Triton X-100). The lysates were cleared by centrifugation and 5 μg of lysate were incubated for 90 min at 37°C with a final concentration of 0.345 mM 4-MU-palmitate (Santa Cruz Biotechnology, Dallas, TX, USA) and 0.03% cardiolipin (w/v, Sigma) in 100 μL reaction buffer. Samples were incubated in the presence and absence of 30 μM Lalstat2 (Sigma), to inhibit LAL activity, and the reaction was quenched with

150 mM EDTA pH 11 (190 μ L). For all 4-MU substrates, fluorescence was measured by using an Tecan Infinite F200 PRO microplate reader (Tecan, Männedorf, Switzerland). with λ_{exc} = 366 nm and λ_{em} = 445 nm.

rhCTSB and rhLAL inhibition assay

Recombinant human CTSB (rhCTSB) was kindly provided by Prof. Paul Saftig and Dr. Alessandro Di Spiezio (University of Kiel). RhCTSB (2 μ g) was pre-incubated for 30 min at RT in 100 μ L of 50 mM sodium acetate, pH 5.5, 0.1 M NaCl, 1 mM EDTA, and 0.2% Triton X-100, for auto-activation of the proCTSB into the mature (active) form of the enzyme. After this period 20 μ M of cathepsin B substrate Z-RR-AMC was added. The POPC and ChA:POPC liposomes were added to this mixture in the indicated concentrations (50, 100, 250, 500, 1000, 1500, 2000 and 2500 μ M) and incubated 30 min on ice. Leupeptin (25 μ M, Sigma, #L2884) was used as a negative control. The samples were incubated 3 h at 37°C for hydrolysis of the substrate to occur. Afterwards the reaction was quenched with 190 μ L with 0.3 M glycine adjusted with NaOH to pH 10.6. Recombinant human LAL (rhLAL, Kanuma®, Sebelipase alfa) was kindly provided by Dr. Eugen Mengel. The rhLAL assay was similar to that described for rhCTSB. Briefly, 100 ng of rhLAL were pre-incubated in assay buffer (100 mM sodium acetate pH 4.0 with 1% Triton X-100) for 30 min at RT. Then the substrate 4MU-palmitate (0.345 mM) was added together with the liposomes and incubated 30 min on ice. Lalistat2 was used as a negative control. Samples were incubated 1 h at 37°C and 190 μ L of 150 mM EDTA pH 11 was used to stop the reaction. The fluorescence was read in a microplate reader MolecularDevices SpectraMax i3x (exc: 360 nm; em: 440 nm).

Treatment with recombinant hydrolases and ZRLR

The cells were incubated for 48 h with the liposomes in coverslips. Afterwards, fresh culture media supplemented with 1 μ g human rhLAL or 5 μ g rhCTSB was added and kept for 24 h. For the CTSB inhibition experiment the cells were treated for 48 h with liposomes in the presence of 100 μ M ZRLR, a specific CTSB

inhibitor kindly provided by Dr. Ewa Wiczerzak (Reich et al., 2009; Wiczerzak et al., 2007). After the mentioned incubations, the cells were fixed with 4% PFA and processed for immunohistochemical analysis.

LLOMe treatment

Cells were cultured in coverslips for 72h in the presence of liposomes, after which 2 mM L-leucyl-L-leucine methyl ester hydrochloride (LLOMe; Bertin, #16008) dissolved in DMSO was added to the culture media and kept for 2 h. DMSO was used as control. The cells were fixed with 4% PFA and processed for immunohistochemical analysis.

Lentiviral plasmids for hTFEB-GFP expression

The plasmid pN1-CMV-TFEB-GFP from Dr. Shawn Ferguson's lab was obtained from Addgene (# 38119). The TFEB-GFP sequence was amplified using primers (Forward: G G G A C A A G T T T G T A C A A A A A G C A G G C T A A A T G G C G T C A C G C A T A G G G T T G C G C A T; Reverse: G G G G A C C A C T T T G T A C A A G A A A G C T G G G T A T T A C T T G T A C A G C T C G T C C A T G C C G A G) containing the attB1/attB2 Gateway® sites. The amplified sequences were cloned into pDONRTM (ThermoScientific) using the Gateway™ BP Clonase™ II enzyme (ThermoScientific). Followed by subcloning subcloned into pLenti6 (ThermoScientific) with the Gateway™ LR Clonase™ II enzyme according to the manufacturer's instructions. All lentiviral particles were produced by co-transfection of pLenti6 and pMD 2.G (VSV-G protein) and psPAX2 (Rev and Pol proteins) into a producer cell line 293STAR RDPro (ATCC). Recombinant viral particles were harvested 48 days later, cleared for cell debris by centrifugation at 3200 g for 10 min and used.

Generation of the hTFEB-GFP overexpressing stable line

Cells were seeded on 6 well format (100 000 cells per well), corresponding to approximately confluency after 24 h. Supernatant of the producer cell line containing the viral particles was added to the cells (500 μ L per well). Antibiotic selection was initiated 72 hours after transduction by replacing the media by culture media supplemented with 10 μ g/mL Blasticidine (Sigma, #15205). After selection, the mixed clone was cultured for two passages after which the population was sorted in a FACS Aria III Cell Sorter. The population with the 2% highest TFEG-GFP signal was selected and cultured in the presence of antibiotic (Gentamicin; Sigma, 1405-41-0) and antifungal (Amphotericin B; ThermoFischer, 15290018) until confluency. After the first passage the cells were cultured in media with Blasticidine, which was removed during the experiments.

TF translocation assay

The cells were cultured in glass coverslips and incubated with liposomes for the indicated period. As positive control the cells were treated with 1 μ M Torin-1 (ApexBio, A8312) or 0.5 μ M Torin-2 (LC Labs, T-8448) in DMSO and added to the cells in culture media without serum.

PI / annexin V staining and LDH assay

Cells were seeded and exposed to ChA or POPC for 48 or 72 h. To detect cell death, annexin V / PI double staining was done with the FITC Annexin V Apoptosis Detection Kit I (BD Biosciences, Sparks, MD, USA) and used according to the standard protocol provided by the supplier. Briefly, after lipids exposure, cells were washed 1x with PBS and incubated with annexin V / PI solution for 30 min, protected from light, in an agitator. Then, images were taken with a Zeiss Axiovert 40 microscope, and PI and annexin V positive cells were counted. As positive control, cells were exposed to 800 μ M of H₂O₂ for 2 h prior to staining.

The activity of the cytoplasmic enzyme lactate dehydrogenase in the supernatant, which evaluates plasma membrane integrity, was determined in VSMCs. After treatment with POPC or ChA for 72 h, the supernatant was collected, and cells were lysed. LDH activity of the supernatant, cell culture media and cell lysates (intracellular content) was determined with the Pierce LDH Cytotoxicity Assay Kit (Thermo Fisher), according to the standard protocol provided by the supplier.

Cell Proliferation evaluation

Cell proliferation was assessed by two different methods. Cell number was assessed by counting the viable cells at each time point, with a Bürker chamber, in the presence of Trypan Blue, a dye exclusion. Cell proliferation was also evaluated by measuring the fluorescence of carboxyfluorescein succinimidyl ester (CFSE) at 48 and 72 h incubation time, in the presence of the lipids. CFSE covalently labels long-lived intracellular molecules with the fluorescent dye. When a CFSE-labeled cell divides, its progeny is endowed with half the number of carboxyfluorescein-tagged molecules and, thus, each cell division can be assessed by measuring the corresponding decrease in cell fluorescence via flow cytometry. In detail, VSMCs were seeded and allowed to grow for 24 h. Then, we used the CellTrace™ CFSE Cell Proliferation Kit (3 µM; ThermoFisher Fisher), following the protocol provided by the supplier. After 48 or 72 h with POPC and ChA, cells were trypsinized and fixed with 4% PFA. CFSE levels were acquired in a BD FACScanto™II flow cytometer: CFSE fluorescence in the 488 nm laser with filter (530/30 BP). The software for acquisition was BD FACSDIVA Diva, and data from at least 5000 cells were analysed with FlowJo. Cellular proliferation is an essential feature of the adaptive immune response. The introduction of the division tracking dye CFSE has made it possible to monitor the number of cell divisions during proliferation and to examine the relationship between proliferation and differentiation.

Western blot

Primary antibodies: anti-LAMP1 (Hybridoma Bank, 1D4B), anti-LC-3 (Sigma, L8918), anti-SQSTM1 (Abnova, H00008878-M0), anti-calnexin (SICGEN, AB0037), anti-cathepsin D (Abcam, ab75852), anti-cathepsin B (R&D Systems, AF965), anti-p21 (Santa Cruz Biotechnology, sc-397), anti-GAPDH (SICGEN, AB0049), anti-mTFEB (Assay Biotech, C10428), anti-hTFEB (Cell Signalling #4240S), anti-phospho-TFEB (Millipore, ABE1971-I), anti-p16-INK4A (Proteintech, 10883-1-AP).

Cell lysates were prepared in lysis buffer (50 mM Tris-HCl, pH 8.0, 1% Triton X-100, 0.5% sodium deoxycholate, 0.1% SDS, 2 mM EDTA, 150 mM NaCl) in the presence of protease inhibitors (Sigma) and phosphatase inhibitor (Calbiochem). Lysates were cleared by centrifugation at 4°C for 30 min at 17,000 × *g* and protein concentrations were determined using the Pierce™ BCA Protein Assay Kit (Thermo Fisher). Samples were then mixed with 4× Laemli buffer (4% SDS, 20% glycerol, 10% 2-mercaptoethanol, 0.004% bromophenol blue and 0.125 M Tris-HCl), heated for 5 min at 95°C and loaded (20-40 µg) on 12-15% SDS polyacrylamide gel. After electrophoresis, proteins were transferred into activated PVDF membranes in transfer buffer 1× (25 mM Tris, 192 mM glycine and 20% methanol) for 75 min, at 300 mA, with gentle agitation. Membranes were then blocked with blocking buffer (5% non-fat dry milk and 0.1% Tween-20 in TBS) for 1 h at room temperature, followed by an ON at 4°C with the primary antibody diluted (1:500-1:1000) in blocking buffer.

After incubation with primary antibodies, membranes were washed with 1× TBS tween and incubated for 1 h at room temperature with the corresponding horseradish peroxidase secondary antibody (Bio-Rad, Hercules, CA, USA) diluted in blocking buffer. Blots were visualized using ECL Prime Western Blot Detection reagent (GE Healthcare) and a Chemidoc Touch Imaging System (Bio-Rad). Bands were quantified using Image Lab 6.0 software (Bio-Rad).

Cycloheximide chase

Cells were cultured for 48h in the presence of ChA liposomes. Afterwards the media was removed and replaced by fresh media with 10 µg/mL cycloheximide (Sigma, C1988) in DMSO. DMSO was used as control. After the mentioned incubation periods (6 or 12 h) the cells were washed and proposed for western blot analysis.

Quantitative RT-PCR

As positive control for the induction of the expression of lysosomal genes, cells were starved for 4 h by incubation with media without serum or treated with 1 µM Torin-1 for 4 h also in media without serum. Total RNA was extracted with NZY total RNA isolation kit (NZYTech, Lisbon, Portugal) and reverse transcription was performed using NZY first-strand cDNA synthesis kit (NZYTech), following the protocol provided by the supplier. Quantitative PCR was performed in a 96 well plate using the SYBR green master mix (NZYtech) using an AB7300 real-time PCR thermal cycler with Step One software (v2.2.2; Applied Biosystems, Waltham, MA, USA) and QuantStudio™ 5 Real-Time PCR System (Thermo Fisher). *gapdh* and *Pgk1* were used as housekeeping genes to normalize the expression. Target gene expression was determined by relative quantification ($\Delta\Delta C_t$ method) to the housekeeping reference gene and the control sample. Primer sequences are indicated in Table S1.

Cytokine release

Supernatant from VSMCs were collected after 72 h of treatment with POPC and ChA. Cytokines levels in the medium were quantified by Mouse IL-6 Uncoated ELISA kit (Invitrogen), according to manufacturer's instructions. Since the number of cells in POPC and ChA-treated cells were different, cytokines levels were normalized to the total cell protein levels, which was quantified as described for the Western blots.

Cell migration and transmigration assays

Cell migration was assessed by wound-healing assay. VSMCs were grown to confluence and 20 mg/ml mitomycin C (Sigma) was added to block the cell cycle 2 h prior to the wound. Cells were wounded by a scratch injury line made with a sterile cell scraper. Cells were then treated with POPC and ChA, and images were taken every 2 h up to 8 h incubation.

For transmigration assays, we used transwell cell culture chambers (Costar, Cambridge, MA, USA) containing filters with 8 μm pore size. VSMCs were treated with POPC and ChA for 72 h and then trypsin-harvested. Chloroquine (Sigma, C6628) was used as positive control for migration inhibition. Cells were suspended in serum-deprived medium and added (1×10^5 cells/well) in the upper chamber of a 24-well plate. Then, complete medium was added to the lower chamber and cells were allowed to transmigrate for 4 h. After incubation, cells were fixed with 4% PFA and stained with 0.1% (w/v) crystal violet in 20% methanol, for 15 min. Cells remaining in the upper chamber of the transwells were removed with a cotton swab and cells that had migrated onto the lower-surface membranes were counted. Images were captured using an Axiovert 40C inverted microscope (Carl Zeiss) equipped with a Powershot A640 digital camera (Canon).

Atomic force microscopy

Cell elasticity was measured using a NanoWizard II atomic force microscope (JPK Instruments, Berlin, Germany) mounted on top of an Axiovert 200 inverted microscope (Carl Zeiss, Jena, Germany). Nanoindentation experiments were carried out on live cells, at 25°C, in Dulbecco's Modified Eagle's Medium (DMEM). Quantitative imaging (QI) mode was used to scan the cells. For these measurements, non-functionalized qp-BioAC CB2 AFM cantilevers (Nanosensors, Neuchâtel, Switzerland) with partial Au coating and quartz-like tips (nominal force constant of 100 pN/nm) were used. Differential interference contrast (DIC) microscopy was used to position the tip on top of the ChA-treated and control cells (only with POPC). QI images of 100 μm \times 100 μm in a z-range of 2.4 μm were acquired. Images of 256 \times 256 pixels with a pixel time of 30 ms

were performed. For every contact between cell and tip, the distance between the cantilever and the cell was adjusted to maintain a maximum applied force of 650 pN before retraction. QI height, adhesion and elasticity images were acquired. Images were analyzed to obtain the cells Young's modulus (E), using JPK Image Processing software v. 6.0.55, by the application of the Hertzian model. AFM tip penetration depth onto cells was also evaluated. This parameter was analyzed by the position of the maximal movement of the piezo sensor in the z-axis, which corresponds to the z-axis coordinate when the sensor reaches an indentation force of 650 pN, subtracting the z-axis position of the sensor when the tip begins the contact with the cell surface. Values above 100 kPa were not considered for the analysis of the stiffness of the cells. A cut-off of values above 1 μm of cell indentation height was also performed for the cell penetration depth images.

Statistical analysis

Data are representative of at least three independent experiments and values depicted on graphs are expressed as mean \pm standard deviation (SD), unless stated otherwise. Statistical analysis (t-test or two-way ANOVA followed by Tukey post-test) was performed using the GraphPad Prism software v. 8.0.2. $p < 0.05$ (*), $p < 0.01$ (**), $p < 0.001$ (***) and $p < 0.0001$ (****) were considered to be statistically significant.

Acknowledgments:

We acknowledge the technical support of the CEDOC Microscopy and Flow cytometry facilities. We would like to thank Dr. Eugen Mengel for providing us with the recombinant LAL and Prof. Paul Saftig and Dr. Alessandro Di Spiezio for the recombinant CTSB. We also thank Dr. Ewa Wiczerzak for the gift of the ZRLR inhibitor, Dr. Miguel Cavadas for the Torin-1 and Dr. Elena Baena for the Torin-2.

Some of the text and Figures 4-8 and some panels of Figures 1-3 and 5 in this paper formed part of Liliana Teresa da Silva Alves' PhD thesis in the Faculdade de Ciências Médicas (NOVA Medical School) at Universidade NOVA de Lisboa and Universidade do Algarve in 2020.

Sources of funding:

This work was supported by Fundação para a Ciência e a Tecnologia, I.P (FCT, Portugal), projects 03/SAICT/2015 and PTDC/MED-PAT/29395/2017, through national funds and co-funded by FEDER under the PT2020 Partnership. The Coimbra Chemistry Centre (CQC) is supported by FCT through project UID/QUI/00313/2019. This work was also supported by Twinning on “Excel in Rare Diseases’ Research: Focus on LYSOsomal Disorders and CILiopathies” (H2020-TWINN-2017: GA 81108). LA was a holder of a FCT PhD fellowship (PD/BD/114254/2016), attributed by the ProRegem Doctoral Programme in 2016. AM was funded by the FCT Stimulus of Scientific Employment Individual Support Call 2017 (CEECIND/01006/2017).

Disclosures:

All authors declare that they do not have any competing interests.

References

- Allahverdian, S., Chaabane, C., Boukais, K., Francis, G. A., & Bochaton-Piallat, M.-L. (2018). Smooth muscle cell fate and plasticity in atherosclerosis. *Cardiovascular Research*, 114(4), 540–550.
- Allahverdian, S., Chehroudi, A. C., McManus, B. M., Abraham, T., & Francis, G. A. (2014). Contribution of intimal smooth muscle cells to cholesterol accumulation and macrophage-like cells in human atherosclerosis. *Circulation*, 129(15), 1551–1559.

- Ameis, D., Merkel, M., Eckerskorn, C., & Greten, H. (1994). Purification, characterization and molecular cloning of human hepatic lysosomal acid lipase. *European Journal of Biochemistry*, 219(3), 905–914.
- Chellan, B., Reardon, C. A., Getz, G. S., & Hofmann Bowman, M. A. (2016). Enzymatically Modified Low-Density Lipoprotein Promotes Foam Cell Formation in Smooth Muscle Cells via Macropinocytosis and Enhances Receptor-Mediated Uptake of Oxidized Low-Density Lipoprotein. *Arteriosclerosis, Thrombosis, and Vascular Biology*, 36(6), 1101–1113.
- Choudhury, A., Dominguez, M., Puri, V., Sharma, D. K., Narita, K., Wheatley, C. L., Marks, D. L., & Pagano, R. E. (2002). Rab proteins mediate Golgi transport of caveola-internalized glycosphingolipids and correct lipid trafficking in Niemann-Pick C cells. *The Journal of Clinical Investigation*, 109(12), 1541–1550.
- Cuervo, A. M., Mann, L., Bonten, E. J., d'Azzo, A., & Dice, J. F. (2003). Cathepsin A regulates chaperone-mediated autophagy through cleavage of the lysosomal receptor. *The EMBO Journal*, 22(1), 47–59.
- de Araujo MEG, Liebscher G, Hess MW, Huber LA. Lysosomal size matters. *Traffic*. 2020;21(1):60-75.
- de Duve, C. (1974). The participation of lysosomes in the transformation of smooth muscle cells to foamy cells in the aorta of cholesterol-fed rabbits. *Acta Cardiologica, Suppl 20*, 9–25.
- di Spiezio, A., Marques, A. R. A., Schmidt, L., Thießen, N., Gallwitz, L., Fogh, J., Bartsch, U., & Saftig, P. (2021). Analysis of cathepsin B and cathepsin L treatment to clear toxic lysosomal protein aggregates in neuronal ceroid lipofuscinosis. *Biochimica et Biophysica Acta. Molecular Basis of Disease*, 1867(10), 166205.
- Ding, Z., Wang, X., Schnackenberg, L., Khaidakov, M., Liu, S., Singla, S., Dai, Y., & Mehta, J. L. (2013). Regulation of autophagy and apoptosis in response to ox-LDL in vascular smooth muscle cells, and the modulatory effects of the microRNA hsa-let-7 g. *International Journal of Cardiology*, 168(2), 1378–1385.
- Domingues, N., Almeida Calado, R. D., Brito, P. H., Matthiesen, R., Ramalho, J., Soares, M. I. L., Pereira, T., Oliveira, L., Vicente, J. R., Wong, L. H., Cho, S. M., Simões, I. C. M., Sampaio, J., Klose, C., Surma, M. A., Almeida, M. S., Rodrigues, G., Araújo-Gonçalves, P., Ferreira, J., ... Vieira, O. v. (2021). Cholesteryl

Hemiazelate Induces Lysosome Dysfunction and Exocytosis in Macrophages. *BioRxiv*, 2021.01.05.422575.

- Domingues, N., Estronca, L. M. B. B., Silva, J., Encarnação, M. R., Mateus, R., Silva, D., Santarino, I. B., Saraiva, M., Soares, M. I. L., Pinho e Melo, T. M. V. D., Jacinto, A., Vaz, W. L. C., & Vieira, O. v. (2017). Cholesteryl hemiesters alter lysosome structure and function and induce proinflammatory cytokine production in macrophages. *Biochimica et Biophysica Acta (BBA) - Molecular and Cell Biology of Lipids*, 1862(2), 210–220.
- Dozynkiewicz, M. A., Jamieson, N. B., Macpherson, I., Grindlay, J., van den Berghe, P. V. E., von Thun, A., Morton, J. P., Gourley, C., Timpson, P., Nixon, C., McKay, C. J., Carter, R., Strachan, D., Anderson, K., Sansom, O. J., Caswell, P. T., & Norman, J. C. (2012). Rab25 and CLIC3 collaborate to promote integrin recycling from late endosomes/lysosomes and drive cancer progression. *Developmental Cell*, 22(1), 131–145.
- Dubland, J. A., Allahverdian, S., Besler, K. J., Ortega, C., Wang, Y., Pryma, C. S., Boukais, K., Chan, T., Seidman, M. A., & Francis, G. A. (2021). Low LAL (Lysosomal Acid Lipase) Expression by Smooth Muscle Cells Relative to Macrophages as a Mechanism for Arterial Foam Cell Formation. *Arteriosclerosis, Thrombosis, and Vascular Biology*, 41(6), e354–e368.
- Estronca, L. M., Silva, J. C., Sampaio, J. L., Shevchenko, A., Verkade, P., Vaz, A. D., Vaz, W. L., & Vieira, O. v. (2012). Molecular etiology of atherogenesis--in vitro induction of lipidosis in macrophages with a new LDL model. *PLoS ONE*, 7(4), e34822.
- Feil, S., Fehrenbacher, B., Lukowski, R., Essmann, F., Schulze-Osthoff, K., Schaller, M., & Feil, R. (2014). Transdifferentiation of vascular smooth muscle cells to macrophage-like cells during atherogenesis. *Circulation Research*, 115(7), 662–667.
- Fowler, S. (1980). Characterization of foam cells in experimental atherosclerosis. *Acta Medica Scandinavica. Supplementum*, 642, 151–158.
- Fowler, S., Berberian, P. A., Shio, H., Goldfischer, S., & Wolinsky, H. (1980). Characterization of cell populations isolated from aortas of rhesus monkeys with experimental atherosclerosis. *Circulation Research*, 46(4), 520–530.

- Geer, J. C., McGILL, H. C. J., & STRONG, J. P. (1961). The fine structure of human atherosclerotic lesions. *The American Journal of Pathology*, 38(3), 263–287.
- Greig, F. H., Kennedy, S., & Spickett, C. M. (2012). Physiological effects of oxidized phospholipids and their cellular signaling mechanisms in inflammation. *Free Radical Biology and Medicine*, 52(2), 266–280.
- Grootaert, M. O. J., Moulis, M., Roth, L., Martinet, W., Vindis, C., Bennett, M. R., & de Meyer, G. R. Y. (2018). Vascular smooth muscle cell death, autophagy and senescence in atherosclerosis. In *Cardiovascular Research* (Vol. 114, Issue 4, pp. 622–634). Oxford University Press.
- Grootaert, M. O., da Costa Martins, P. A., Bitsch, N., Pintelon, I., de Meyer, G. R., Martinet, W., & Schrijvers, D. M. (2015). Defective autophagy in vascular smooth muscle cells accelerates senescence and promotes neointima formation and atherogenesis. *Autophagy*, 11(11), 2014–2032.
- Hemesath, T. J., Steingrímsson, E., McGill, G., Hansen, M. J., Vaught, J., Hodgkinson, C. A., Arnheiter, H., Copeland, N. G., Jenkins, N. A., & Fisher, D. E. (1994). microphthalmia, a critical factor in melanocyte development, defines a discrete transcription factor family. *Genes & Development*, 8(22), 2770–2780.
- Hill, J. W., & Carothers, W. H. (1933). Studies of Polymerization and Ring Formation. XIX. Many-Membered Cyclic Anhydrides. *Journal of the American Chemical Society*, 55(12), 5023–5031.
- Hipolito, V. E. B., Diaz, J. A., Tandoc, K. v, Oertlin, C., Ristau, J., Chauhan, N., Saric, A., Mclaughlan, S., Larsson, O., Topisirovic, I., & Botelho, R. J. (2019). Enhanced translation expands the endo-lysosome size and promotes antigen presentation during phagocyte activation. *PLoS Biology*, 17(12), e3000535.
- Huang, T. C., Chen, C. P., Wefler, V., & Raftery, A. (1961). A Stable Reagent for the Liebermann-Burchard Reaction: Application to Rapid Serum Cholesterol Determination. *Analytical Chemistry*, 33(10), 1405–1407.
- Jerome, W G, & Lewis, J. C. (1985). Early atherogenesis in White Carneau pigeons. II. Ultrastructural and cytochemical observations. *The American Journal of Pathology*, 119(2), 210–222.
- Jerome, W. G., Minor, L. K., Glick, J. M., Rothblat, G. H., & Lewis, J. C. (1991). Lysosomal lipid accumulation in vascular smooth muscle cells. *Experimental and Molecular Pathology*, 54(2), 144–158.

- Jerome, W. Gray, & Lewis, J. C. (1990). Early atherogenesis in white carneau pigeons: Effect of a short-term regression diet. *Experimental and Molecular Pathology*, 53(3), 223–238.
- Kim, J., Kundu, M., Viollet, B., & Guan, K.-L. (2011). AMPK and mTOR regulate autophagy through direct phosphorylation of Ulk1. *Nature Cell Biology*, 13(2), 132–141.
- Klein, B., Kleinman, N. B. & Foreman, J. A. Preparation and evaluation of a water-soluble cholesterol standard. *Clinical chemistry* 20, 482-485 (1974).
- Lu, S., Sung, T., Lin, N., Abraham, R. T., & Jessen, B. A. (2017). Lysosomal adaptation: How cells respond to lysosomotropic compounds. *PloS One*, 12(3), e0173771. Maejima, I., Takahashi, A., Omori, H., Kimura, T., Takabatake, Y., Saitoh, T., Yamamoto, A., Hamasaki, M., Noda, T., Isaka, Y., & Yoshimori, T. (2013). Autophagy sequesters damaged lysosomes to control lysosomal biogenesis and kidney injury. *The EMBO Journal*, 32(17), 2336–2347.
- Marques, A. R. A., di Spiezio, A., Thießen, N., Schmidt, L., Grötzinger, J., Lüllmann-Rauch, R., Damme, M., Storck, S. E., Pietrzik, C. U., Fogh, J., Bär, J., Mikhaylova, M., Glatzel, M., Bassal, M., Bartsch, U., & Saftig, P. (2019). Enzyme replacement therapy with recombinant pro-CTSD (cathepsin D) corrects defective proteolysis and autophagy in neuronal ceroid lipofuscinosis. *Autophagy*, 1–15.
- Marques, A. R. A., Ramos, C., Machado-Oliveira, G., & Vieira, O. v. (2021). Lysosome (Dys)function in Atherosclerosis-A Big Weight on the Shoulders of a Small Organelle. *Frontiers in Cell and Developmental Biology*, 9, 658995.
- Martina, J. A., Diab, H. I., Brady, O. A., & Puertollano, R. (2016). TFEB and TFE3 are novel components of the integrated stress response. *The EMBO Journal*, 35(5), 479–495.
- Matthiesen, R., Lauber, C., Sampaio, J. L., Domingues, N., Alves, L., Gerl, M. J., Almeida, M. S., Rodrigues, G., Araújo Gonçalves, P., Ferreira, J., Borbinha, C., Pedro Marto, J., Neves, M., Batista, F., Viana-Baptista, M., Alves, J., Simons, K., Vaz, W., & Vieira, O. V. (2021). Shotgun mass spectrometry-based lipid profiling identifies and distinguishes between chronic inflammatory diseases. *EBioMedicine*, 70, 103504.

- Mauthe, M., Orhon, I., Rocchi, C., Zhou, X., Luhr, M., Hijlkema, K.-J., Coppes, R. P., Engedal, N., Mari, M., & Reggiori, F. (2018). Chloroquine inhibits autophagic flux by decreasing autophagosome-lysosome fusion. *Autophagy*, *14*(8), 1435–1455.
- Maxson, M. E., & Grinstein, S. (2014). The vacuolar-type H⁺-ATPase at a glance - more than a proton pump. *Journal of Cell Science*, *127*(23), 4987–4993.
- Medina, D. L., di Paola, S., Peluso, I., Armani, A., de Stefani, D., Venditti, R., Montefusco, S., Scotto-Rosato, A., Prezioso, C., Forrester, A., Settembre, C., Wang, W., Gao, Q., Xu, H., Sandri, M., Rizzuto, R., de Matteis, M. A., & Ballabio, A. (2015). Lysosomal calcium signalling regulates autophagy through calcineurin and TFEB. *Nature Cell Biology*, *17*(3), 288–299.
- Mindell, J. A. (2012). Lysosomal Acidification Mechanisms. *Annual Review of Physiology*, *74*(1), 69–86.
- Minor, L. K., Mahlberg, F. H., Jerome, W. G., Lewis, J. C., Rothblat, G. H., & Glick, J. M. (1991). Lysosomal hydrolysis of lipids in a cell culture model of smooth muscle foam cells. *Experimental and Molecular Pathology*, *54*(2), 159–171.
- Monteiro, P., Rossé, C., Castro-Castro, A., Irondelle, M., Lagoutte, E., Paul-Gilloteaux, P., Desnos, C., Formstecher, E., Darchen, F., Perrais, D., Gautreau, A., Hertzog, M., & Chavrier, P. (2013). Endosomal WASH and exocyst complexes control exocytosis of MT1-MMP at invadopodia. *The Journal of Cell Biology*, *203*(6), 1063–1079.
- Nakatogawa, H. (2020). Mechanisms governing autophagosome biogenesis. *Nature Reviews Molecular Cell Biology*, *21*(8), 439–458.
- Napolitano, G., & Ballabio, A. (2016). TFEB at a glance. *Journal of Cell Science*, *129*(13), 2475–2481.
- Newby, A. C., & Zaltsman, A. B. (1999). Fibrous cap formation or destruction - The critical importance of vascular smooth muscle cell proliferation, migration and matrix formation. In *Cardiovascular Research* (Vol. 41, Issue 2, pp. 345–360). Oxford Academic.
- Pan, H.-Y., Alamri, A. H., & Valapala, M. (2019). Nutrient deprivation and lysosomal stress induce activation of TFEB in retinal pigment epithelial cells. *Cellular & Molecular Biology Letters*, *24*, 33.

- Reich, M., Wiczerzak, E., Jankowska, E., Palesch, D., Boehm, B. O., & Burster, T. (2009). Specific cathepsin B inhibitor is cell-permeable and activates presentation of TTC in primary human dendritic cells. *Immunology Letters*, 123(2), 155–159.
- Saffi, G. T., & Botelho, R. J. (2019). Lysosome Fission: Planning for an Exit. *Trends in Cell Biology*, 29(8), 635–646.
- Santarino, I. B., Viegas, M. S., Domingues, N. S., Ribeiro, A. M., Soares, M. P., & Vieira, O. v. (2017). Involvement of the p62/NRF2 signal transduction pathway on erythrophagocytosis. *Scientific Reports*, 7(1), 5812.
- Sergin, I., Evans, T. D., Zhang, X., Bhattacharya, S., Stokes, C. J., Song, E., Ali, S., Dehestani, B., Holloway, K. B., Micevych, P. S., Javaheri, A., Crowley, J. R., Ballabio, A., Schilling, J. D., Epelman, S., Weihl, C. C., Diwan, A., Fan, D., Zayed, M. A., & Razani, B. (2017). Exploiting macrophage autophagy-lysosomal biogenesis as a therapy for atherosclerosis. *Nature Communications*, 8, 15750.
- Settembre, C., Fraldi, A., Medina, D. L., & Ballabio, A. (2013). Signals from the lysosome: A control centre for cellular clearance and energy metabolism. In *Nature Reviews Molecular Cell Biology*, 14(5), 283–296.
- Shankman, L. S., Gomez, D., Cherepanova, O. A., Salmon, M., Alencar, G. F., Haskins, R. M., Swiatlowska, P., Newman, A. A. C., Greene, E. S., Straub, A. C., Isakson, B., Randolph, G. J., & Owens, G. K. (2015). KLF4-dependent phenotypic modulation of smooth muscle cells has a key role in atherosclerotic plaque pathogenesis. *Nature Medicine*, 21(6), 628–637.
- Sharma, D. K., Choudhury, A., Singh, R. D., Wheatley, C. L., Marks, D. L., & Pagano, R. E. (2003). Glycosphingolipids internalized via caveolar-related endocytosis rapidly merge with the clathrin pathway in early endosomes and form microdomains for recycling. *The Journal of Biological Chemistry*, 278(9), 7564–7572.
- Shio, H., Haley, N. J., & Fowler, S. (1979). Characterization of lipid-laden aortic cells from cholesterol-fed rabbits. III. Intracellular localization of cholesterol and cholesteryl ester. *Laboratory Investigation; a Journal of Technical Methods and Pathology*, 41(2), 160–167.
- Vengrenyuk, Y., Nishi, H., Long, X., Ouimet, M., Savji, N., Martinez, F. O., Cassella, C. P., Moore, K. J., Ramsey, S. A., Miano, J. M., & Fisher, E. A. (2015). Cholesterol loading reprograms the microRNA-143/145-myocardin axis to convert aortic

- smooth muscle cells to a dysfunctional macrophage-like phenotype. *Arteriosclerosis, Thrombosis, and Vascular Biology*, 35(3), 535–546.
- Viegas, M. S., Estronca, L. M., & Vieira, O. v. (2012). Comparison of the kinetics of maturation of phagosomes containing apoptotic cells and IgG-opsionized particles. *PLoS ONE*, 7(10), e48391.
- Wang, Y., Dubland, J. A., Allahverdian, S., Asonye, E., Sahin, B., Jaw, J. E., Sin, D. D., Seidman, M. A., Leeper, N. J., & Francis, G. A. (2019). Smooth Muscle Cells Contribute the Majority of Foam Cells in ApoE (Apolipoprotein E)-Deficient Mouse Atherosclerosis. *Arteriosclerosis, Thrombosis, and Vascular Biology*, 39(5), 876–887.
- Wieczerek, E., Rodziewicz-Motowidło, S., Jankowska, E., Gieldoń, A., & Ciarkowski, J. (2007). An enormously active and selective azapeptide inhibitor of cathepsin B. *Journal of Peptide Science: An Official Publication of the European Peptide Society*, 13(8), 536–543.
- Wolinsky, H., Goldfischer, S., Schiller, B., & Kasak, L. E. (1974). Modification of the effects of hypertension on lysosomes and connective tissue in the rat aorta. *Circulation Research*, 34(2), 233–241.
- Xu, K., Yang, Y., Yan, M., Zhan, J., Fu, X., & Zheng, X. (2010). Autophagy plays a protective role in free cholesterol overload-induced death of smooth muscle cells. *Journal of Lipid Research*, 51(9), 2581–2590.
- Yancey, P. G., & Jerome, W. G. (1998). Lysosomal sequestration of free and esterified cholesterol from oxidized low density lipoprotein in macrophages of different species. *Journal of Lipid Research*, 39(7), 1349–1361.
- Zschenker, O., Oezden, D., & Ameis, D. (2004). Lysosomal acid lipase as a preproprotein. *Journal of Biochemistry*, 136(1), 65–72.

Figures

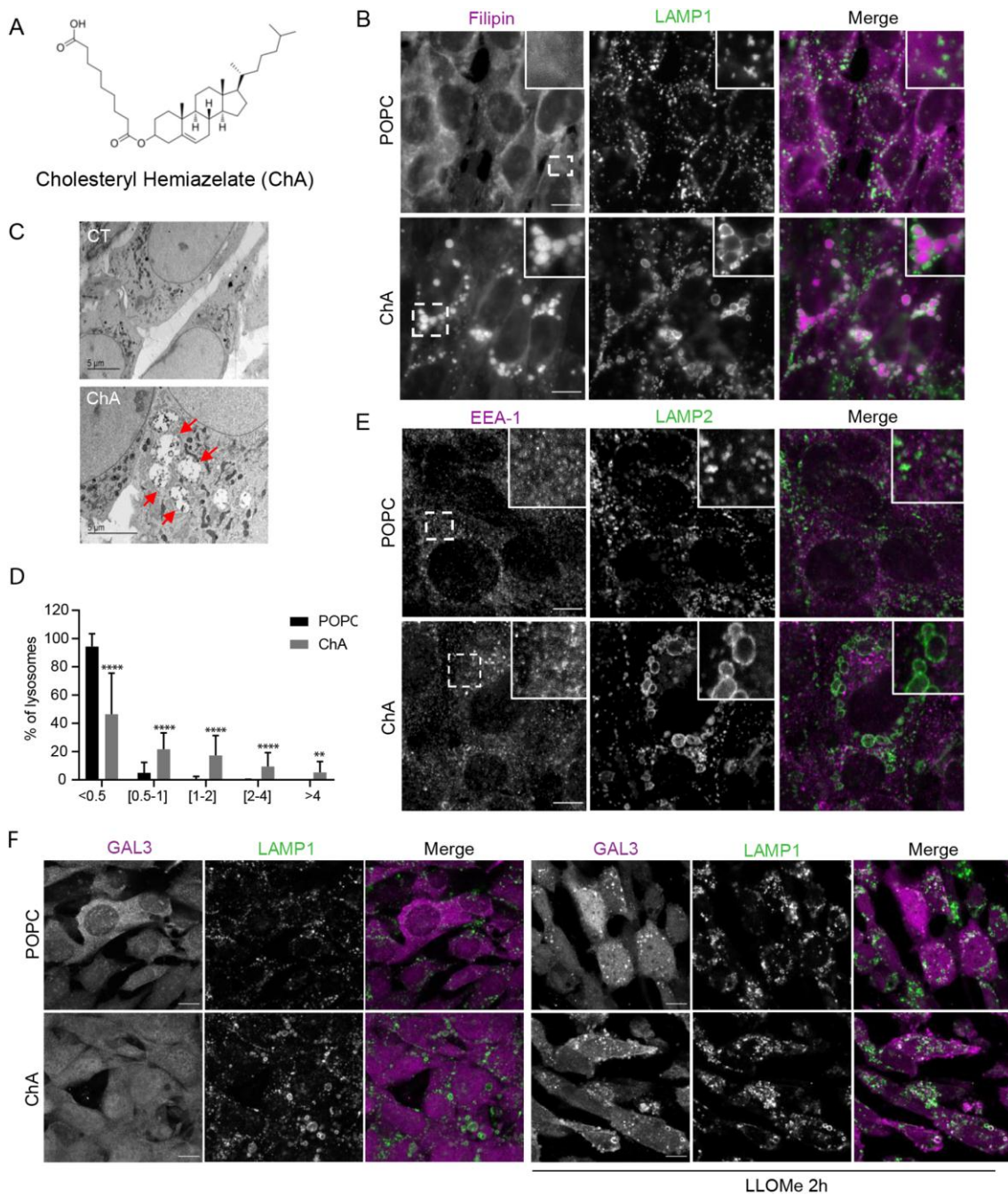


Figure 1: Impact of ChA in lysosome morphology and integrity. (A) Cholesteryl hemiazelate (ChA) chemical structure; (B) VSMCs were treated with ChA or the vehicle-POPC for 72h. Representative images of VSMCs labelled with filipin (a free cholesterol and ChA probe, magenta) and LAMP1 (green). Insets represent zooms of the regions outlined by the dashed

rectangles. Confocal single-slice images magnification: 63x; scale bar: 10 μm . **(C)** Transmission electron microscopy of control cells or treated for 72 h with ChA. Scale bar: 5 μm . Enlarged lysosomes are indicated by red arrows. **(D)** Percentage of LAMP2-positive organelles (i.e. lysosomes) as a function of individual LAMP2-positive organelle area in POPC and ChA treated cells. Data represent the mean \pm SD of 3 independent experiments. Statistical significance was assessed by 2way ANOVA by Sidak's multiple comparisons test: **, $p < 0.01$; ****, $p < 0.0001$. **(E)** Representative images of VSMCs stained with EEA-1 (magenta) and LAMP2 (green). Insets represent zooms of the regions outlined by the dashed rectangles. Confocal single-slice images magnification: 63x; scale bar: 10 μm . **(F)** VSMCs were treated with POPC or ChA liposomes for 72h (left panel) and then with lysosomal membrane permeabilization (LMP) agent LLOMe for 2 h (right panel). Representative images of cells stained with antibodies against Galectin-3 (Gal3, magenta) and LAMP1 (green). Confocal single-slice images magnification: 63x; scale bar: 10 μm .

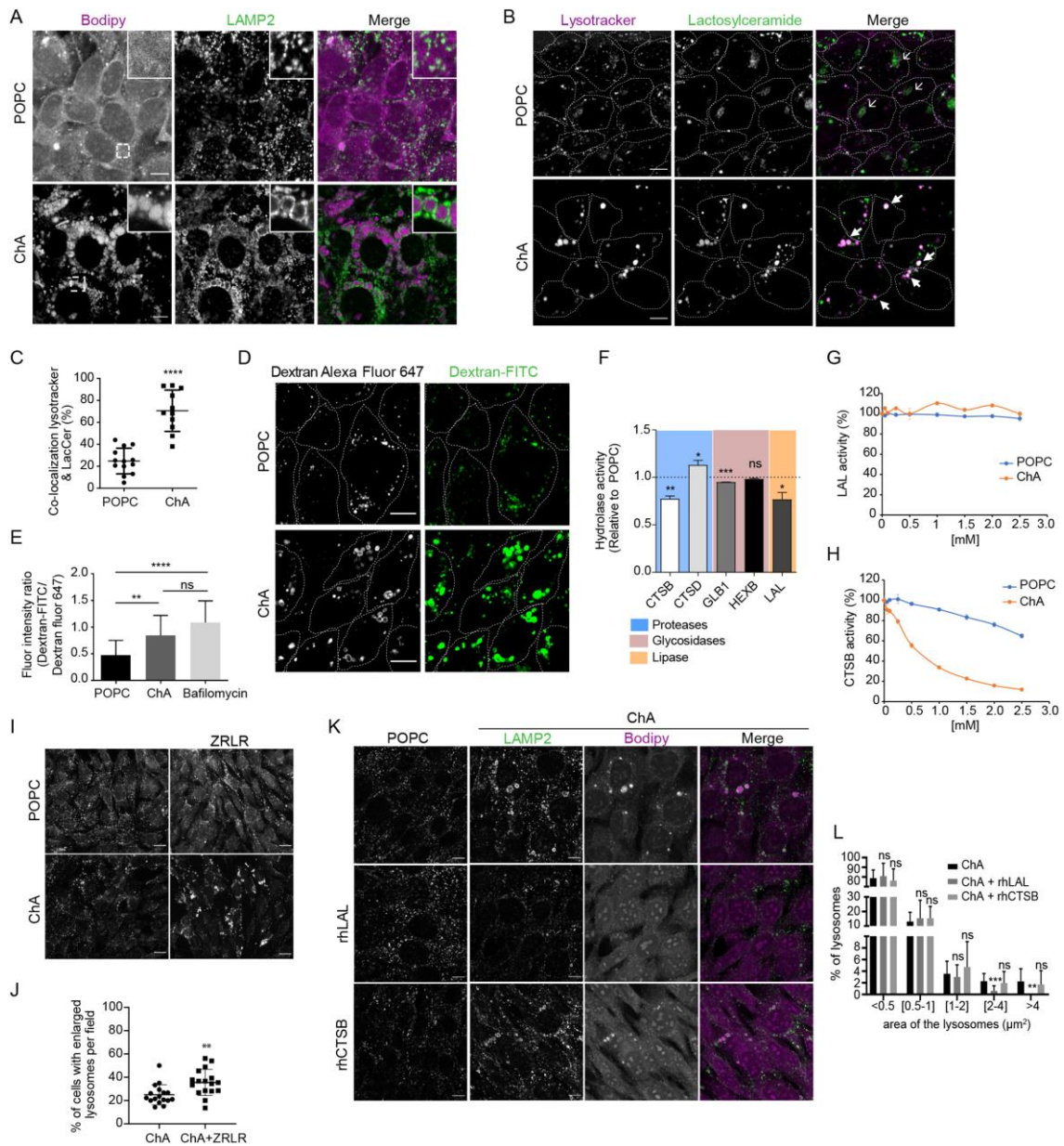


Figure 2: Exposure of VSMCs to ChA triggers neutral lipid accumulation, impairs lysosome acidification and hydrolase activity. (A) VSMCs were incubated for 72h with POPC or ChA. After incubation, cells were labelled with LAMP2 (green) and Bodipy 493/503 (neutral lipids dye; magenta). Insets represent zooms of the regions outlined by the dashed rectangles. Confocal single-slice images with magnification: 63x; scale bar: 10 μm . **(B)** Representative images of 72h ChA-treated VSMCs incubated with Lysotracker (magenta) and lactosylceramide (green) and, then, chased for 3h. At this time-point, VSMCs treated with POPC show that most of the internalized

lactosylceramide already reached the Golgi (thin arrow), in comparison with VSMCs treated with ChA, where the lipid remained in acidic organelles (thick arrow). Confocal single-slice images magnification: 63x; scale bar: 10 μ m. Dashed lines indicate the cell border. **(C)** Percentage of co-localization of lactosylceramide-positive organelles with LysoTracker in cells treated with POPC and ChA for 72h, after 3h of chase. Data represent the mean \pm SD of 3 independent experiments. Statistical significance was assessed by unpaired t-test: ****, $p < 0.0001$. **(D)** After VSMCs were treated with POPC or ChA for 72h, cells were loaded with dextran-FITC (pH sensitive probe; gray) and dextran-Alexa fluor 647 (pH insensitive probe; green). Confocal single-slice images magnification: 63x; scale bar: 10 μ m. Dashed line indicates cell border. **(E)** Quantification of the fluorescence emission (mean intensity) ratio of dextran-FITC and dextran-Alexa Fluor 647. ImageJ software was applied, and more than 32 cells were quantified. Data represent the mean \pm SD of 3 independent experiments. Statistical significance was assessed by unpaired t-test: **, $p < 0.01$. **(F)** Measurement of the *in vitro* activity of lysosomal hydrolases in ChA-treated cells normalized to POPC-treated cells (dashed line). Data represent the mean \pm SD of 3 independent experiments. Statistical significance was assessed by unpaired t-test: *, $p < 0.05$; **, $p < 0.01$; ***, $p < 0.001$; ns, non-significant. **(G)** *In vitro* activity of rhLAL towards the artificial substrate in the presence of increasing concentrations of POPC or ChA liposomes (50 to 2500 μ M). Activity relative to rhLAL in the absence of liposomes. Data represent the mean \pm SD of 3 replicates. **(H)** *In vitro* activity of rhCTSB towards the artificial substrate in the presence of increasing concentrations of POPC or ChA liposomes (50 to 2500 μ M). Activity relative to rhCTSB in the absence of liposomes. Data represent the mean \pm SD of 3 replicates. **(I)** VSMCs were treated for 48h with liposomes in the presence or absence of 100 μ M of the CT SB inhibitor ZRLR. Representative images of VSMCs stained with anti-LAMP1 antibody. Scale bar = 20 μ m. **(J)** Quantification of the percentage of cells per field showing lysosomal enlargement. Data represent the mean \pm SD of 3 independent experiments. Per experiment 7 fields were analysed. Statistical significance was assessed by unpaired t-test: **, $p < 0.01$. **(K)** VSMCs were incubated for 48h with ChA or POPC and then for 24h with rhLAL or rhCTSB. Representative images of VSMCs stained with anti-LAMP1 (green) antibody and labelled with Bodipy

493/503 (magenta). Confocal single-slice images magnification: 63x; scale bar: 10 μm . **(L)** Percentage of LAMP1-positive organelles (i.e. lysosomes) as a function of individual LAMP1-positive organelle area in cells treated with ChA for 48 h followed by treatment with rhLAL or rhCTSB for 24h. Data represent the mean \pm SD of 3 independent experiments. Statistical significance was assessed by 2way ANOVA by Sidak's multiple comparisons test: **, $p < 0.01$; ***, $p < 0.001$.

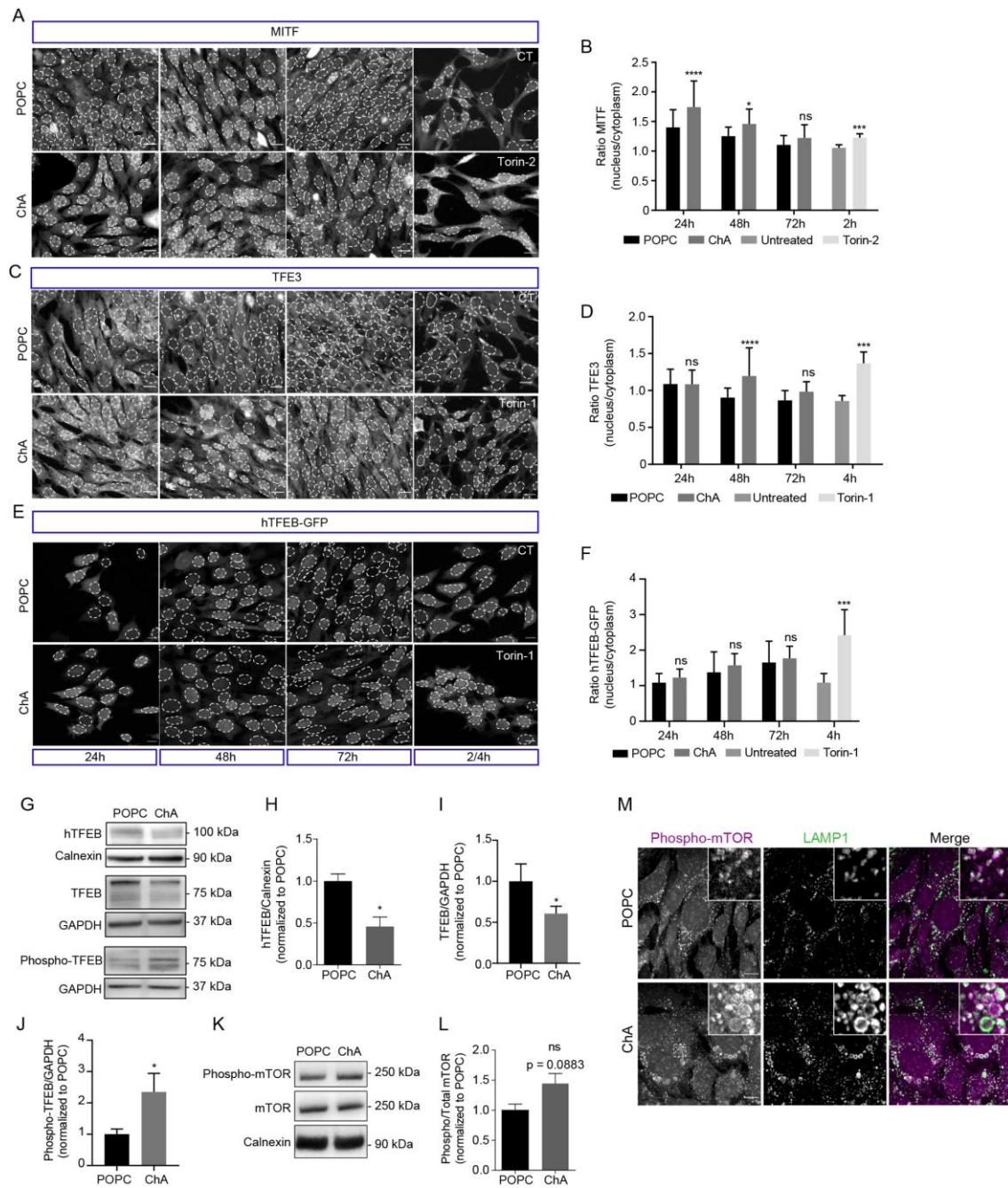


Figure 3: ChA leads to the nuclear translocation of MITF and TFE3 but not TFEB. VSMCs were incubated for 24, 48 or 72h with POPC or ChA. Torin-2 (2h incubation) was used as positive control for MITF translocation and Torin-1 (4h incubation) as a positive control for TFE3 and hTFEB-GFP translocation. After incubation, cells were probed with antibodies directed against MITF (**A**) or TFE3 (**C**). Fluorescence microscopy images of MITF and TFE3 (Zeiss Axio Imager Z2 microscope). Magnification: 63x; scale bar: 20 μ m. TFEB was visualized via the

GFP protein fused at the C-terminus of hTFEB **(E)**. Confocal microscopy pictures of hTFEB-GFP (Zeiss LSM980). Magnification: 63x; scale bar: 20 μm . Nucleus delimited by dashed lines. **(B)**, **(D)** and **(F)** represent the ratio of mean intensity of MITF, TFE3 and TFEB-GFP fluorescence, respectively, of the nucleus with cytoplasm at 24, 48 and 72 h in cells treated with POPC and ChA. Data represent the mean \pm SD of 3 independent experiments. Statistical significance was assessed by two-way ANOVA, SIDAK test: *, $p < 0.05$; ***, $p < 0.001$; ****, $p < 0.0001$; ns, non-significant. **(G)** Western blot for hTFEB in lysates of a VSMC stable cell line overexpressing hTFEB-GFP treated with POPC or ChA for 72 h. Calnexin was used as loading control. TFEB and phospho-TFEB in lysates of (wild-type) VSMCs treated with POPC and ChA for 72 h. GAPDH was used as loading control. Densiometric quantification of the hTFEB-GFP/Calnexin **(H)**, TFEB-GFP/GAPDH **(I)** and phospho-TFEB-GFP/GAPDH **(J)** western blot band ratio. Data represent the mean \pm SD of 3 independent experiments. Statistical significance was assessed by unpaired t-test: *, $p < 0.05$. **(K)** Western blot for total and phospho-mTOR in lysates of VSMCs treated with POPC or ChA for 72h. Calnexin was used as a loading control. **(L)** Densiometric quantification of the Phospho/Total-mTOR western blot band ratio (normalized to calnexin). Data represent the mean \pm SD of 3 independent experiments. Statistical significance was assessed by unpaired t-test: $p = 0.0883$. **(M)** VSMCs were incubated for 72h with POPC or ChA liposomes. Representative images of VSMCs immunostained with anti-LAMP1 (green) or anti-phospho-mTOR (magenta) antibodies. Insets represent zooms of the regions outlined by the dashed rectangles. Confocal single-slice images magnification: 63x; scale bar: 10 μm .

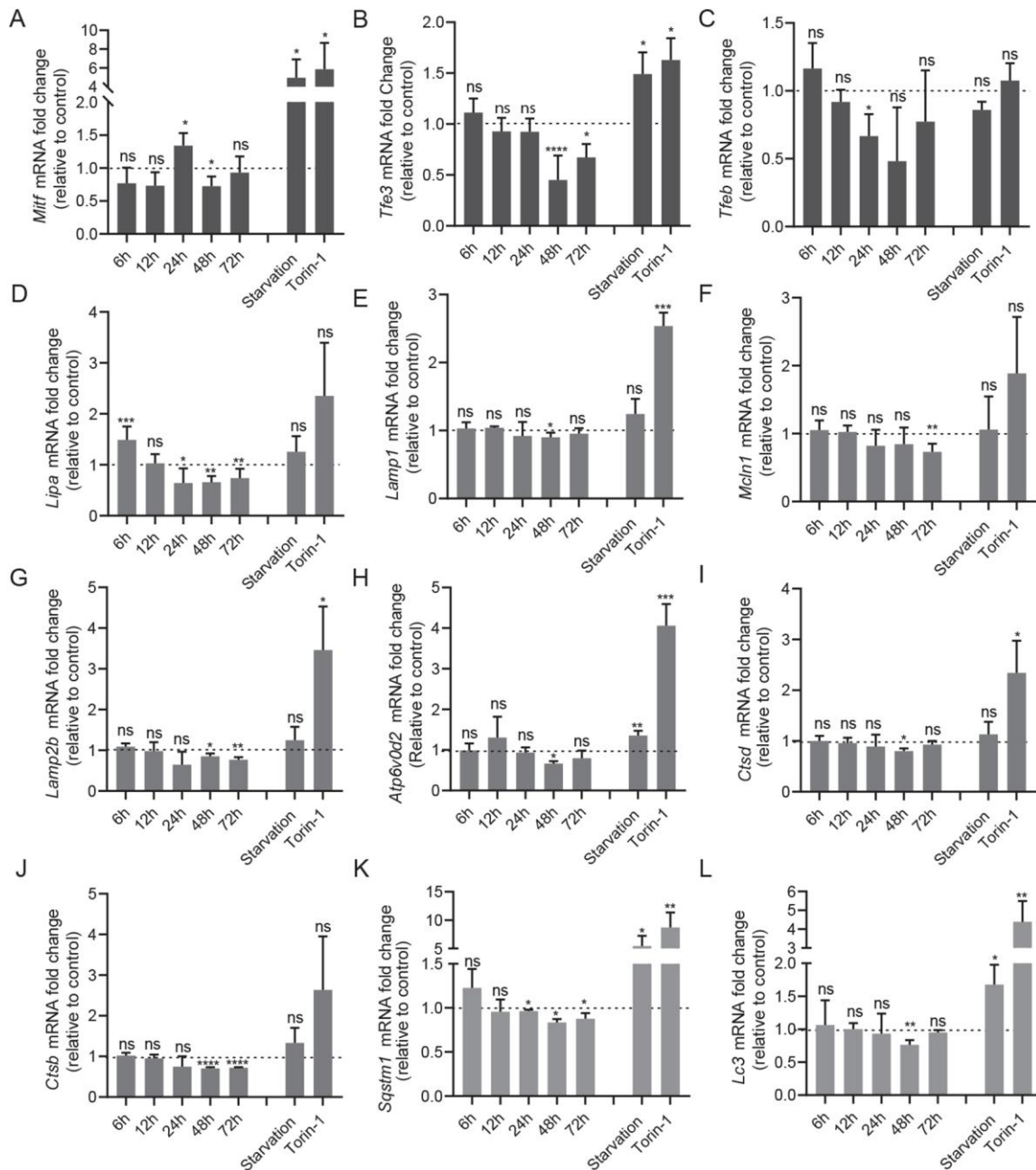


Figure 4: ChA does not induce transcription of lysosomal and autophagic genes. VSMCs were incubated with POPC or ChA for 6, 12, 24, 48 and 72h, and mRNA was extracted and analysed by RT-qPCR for the transcription factors *Mitf* (A), *Tfe3* (B), *Tfeb* (C), and their effectors *Lipa* (D), *Lamp1* (E), *Mcln1* (F), *Lamp2b* (G), *Atp6v0d2* (H), *cathepsin D* (I) and *cathepsin B* (J); for autophagy evaluation mRNA was analysed for *Sqstm1* (K) and *lc3* (L). Starvation or Torin-1 treatment (both for 4h) were used as positive controls. Data were normalized to the endogenous *Gapdh* and *Pgk1* genes. Data

represent the mean \pm SD of 3 independent experiments. Statistical significance was assessed by unpaired t-test: *, $p < 0.05$; **, $p < 0.01$; ****, $p < 0.0001$; ns, non-significant. Data is normalized to POPC levels (dashed line).

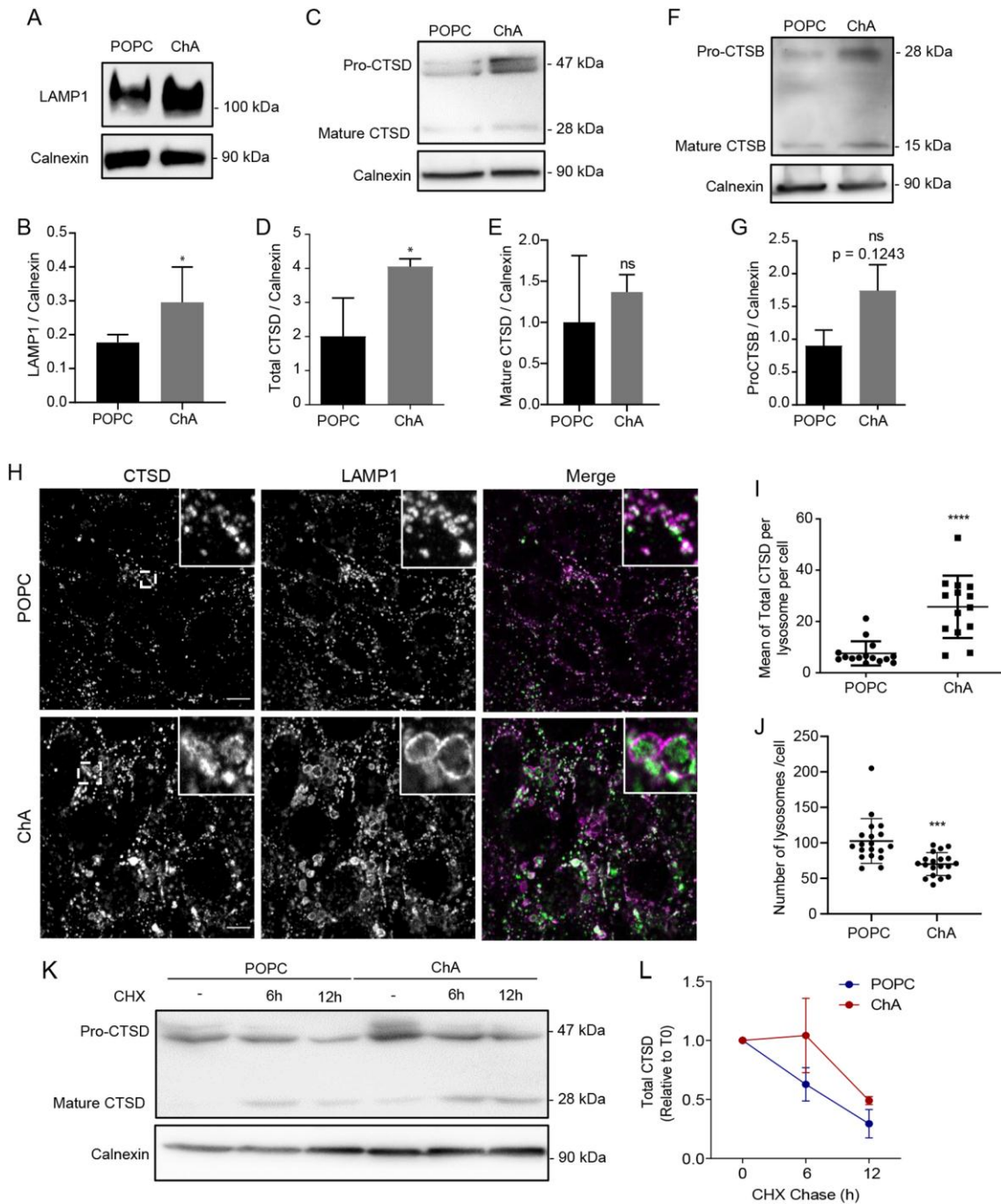


Figure 5: ChA increases lysosomal mass and impairs the maturation of lysosomal zymogen hydrolases in VSMCs. (A), (C) and (F) represent LAMP1, cathepsin D (CTSD) and cathepsin B (CTSB) protein levels (assessed by western blot), respectively, in VSMCs treated with POPC or ChA for 72h. Calnexin was used as loading control. (B), (D), (E) and (G), represent the ratios of LAMP1/calnexin, total (pro- plus mature) CTSD/calnexin, mCTSD/calnexin and pro-CTSB/calnexin, respectively, of quantified western blot bands. (B), (D)

and **(E)** represent the mean \pm SD of 3 independent experiments, and **(G)** represents the mean \pm SD of 2 independent experiments. Statistical significance was assessed by student t-test: *, $p < 0.05$; ns, non-significant. **(H)** Representative images of VSMCs incubated for 72h with POPC or ChA. After incubation, cells were co-stained with cathepsin D (green) and LAMP1 (magenta) antibodies. Insets represent zooms of the regions outlined by the dashed rectangles. Confocal single-slice images magnification: 63x; scale bar: 10 μm . **(I)** Quantification of total CTSD per lysosome per cell in POPC and ChA treated cells. Data represents the mean \pm SD of 15 cells of 3 independent experiments. Statistical significance was assessed by unpaired t-test: ****, $p < 0.0001$. **(J)** Number of lysosomes per cell in VSMCs treated with POPC or ChA at 72 h. Data represent the mean \pm SD of 19 or more cells of 3 independent experiments. Statistical significance was assessed by unpaired t-test: *, $p < 0.05$. **(K)** VSCMs were treated for 48h with POPC or ChA and afterwards a 6 or 12 h chase with cycloheximide (CHX) was performed. The cell lysates were analysed by western blot with antibodies against CTSD using calnexin as loading control. **(L)** Densitometric quantification of the total CTSD (sum of pro- and mature forms) normalized to calnexin levels and relative to $t=0$ for each condition (POPC and ChA). Data represent the mean \pm SD of 3 independent experiments. Statistical significance was assessed by student t-test (non-significant).

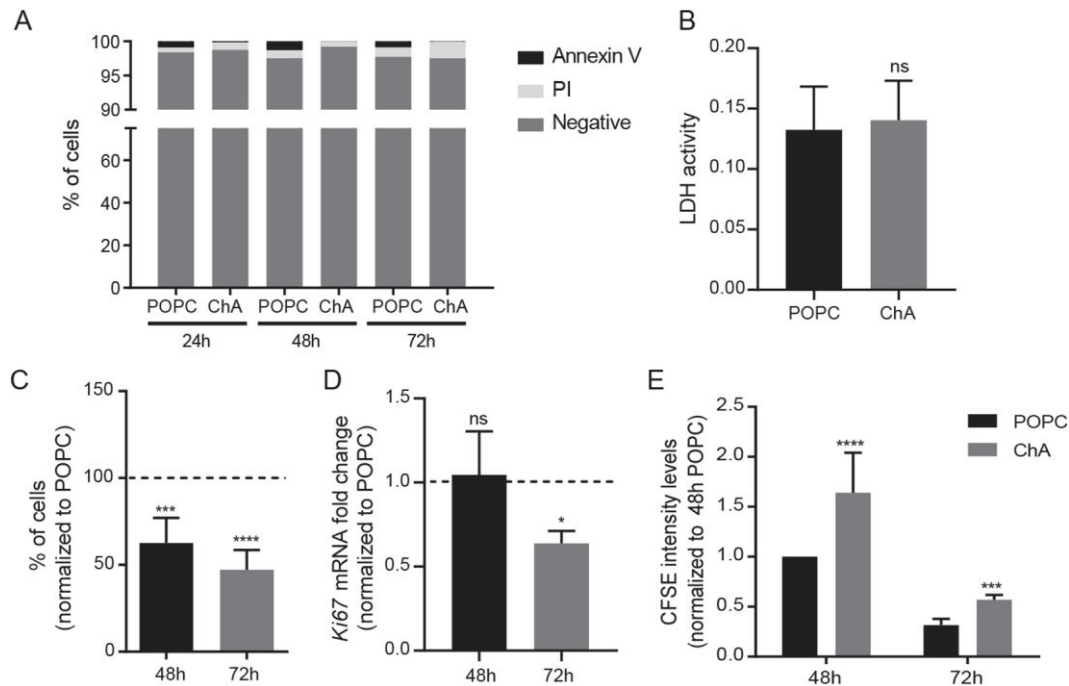


Figure 6: ChA delays VSMCs proliferation rate. (A) Percentage of cells without staining (negative), necrotic (PI positive) and apoptotic (annexin V positive) after 24, 48 and 72h of treatment (POPC or ChA). All conditions were repeated 3 times and more than 500 cells were analysed per condition. **(B)** Quantification of LDH activity from the medium of POPC and ChA treated cells after 72h of treatment. Data represent the mean \pm SD of 3 independent experiments. Statistical significance was assessed two-way NOVA: ns, non-significant. **(C)** Percentage of cell number at 48 and 72h after POPC and ChA treatment. Values normalized to POPC (100%). Data represent the mean \pm SD of 3 independent experiments. Statistical significance was assessed by two-way ANOVA: ***, $p < 0.001$; ****, $p < 0.0001$. **(D)** VSMCs *Ki-67* mRNA expression evaluated by RT-qPCR at 48 and 72h of exposure to POPC and ChA. Data were normalized to the endogenous *Gapdh* and *Pgk1* genes. Data represent the mean \pm SD of 3 independent experiments and were normalized to POPC (dashed line). Statistical significance was assessed by two-way ANOVA: *, $p < 0.05$; ns, non-significant. **(E)** CFSE intensity levels in VSMCs after a pulse of 20 min of CFSE and a chase of 48 or 72h with POPC or ChA treatment. Data represent the mean \pm SD of 5 independent experiments and were normalized to POPC at 48 h. Statistical significance was assessed by unpaired t-test: ***, $p < 0.001$; ****, $p < 0.0001$.

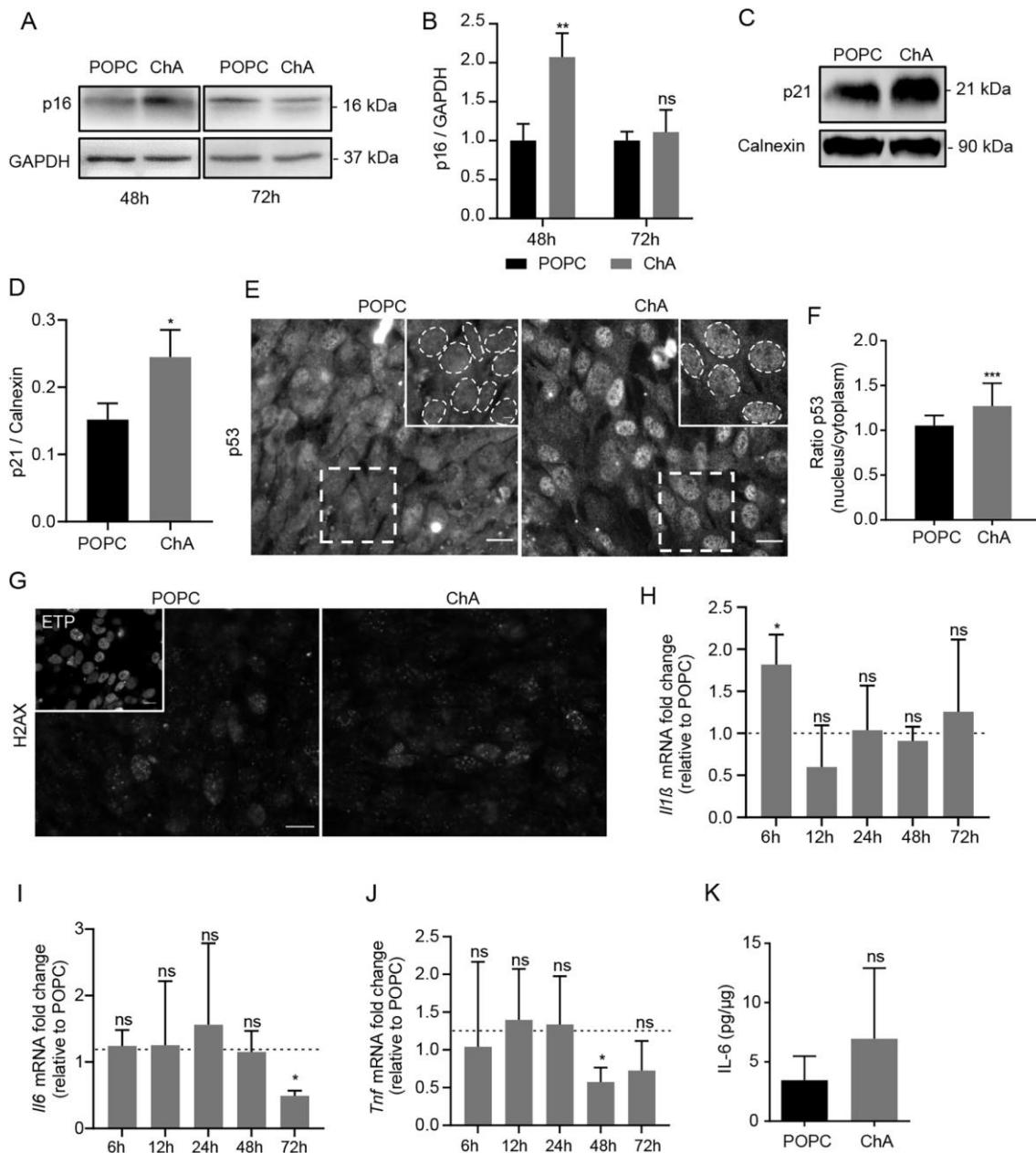


Figure 7: ChA-treated VSMCs show an increase of early senescent-like markers. **(A)** Western blot for p16 of VSMCs treated with POPC and ChA at 48 and 72h. GAPDH was used as loading control. **(B)** p16/GAPDH ratio of bands obtained by Western blot in **(A)**. Data represent the mean \pm SD of 3 independent experiments. Statistical significance was assessed by unpaired t-test: **, $p < 0.01$; ns, non-significant. **(C)** Western blot for p21 levels in VSMCs treated with POPC and ChA for 72 h. Calnexin was used as loading control. **(D)** p21/calnexin ratio of quantified bands obtained in **(C)**. Data represent the mean \pm SD of 3 independent experiments. Statistical significance was assessed by

unpaired t-test: **, $p < 0.01$; ns, non-significant. **(E)** VSMCs were incubated 72h with POPC or ChA. After incubation, cells were stained for p53. Fluorescence microscopy images (Zeiss Axio Imager Z2 microscope); nucleus delimited by dashed lines. Magnification: 63x; scale bar: 20 μm . **(F)** Ratio of mean fluorescence intensities of p53 in the nucleus and cytoplasm at 72 h in cells treated with POPC and ChA. Data represent the mean \pm SD of 3 independent experiments. Statistical significance was assessed by unpaired t-test: ***, $p < 0.001$. **(G)** VSMCs incubated 72h with POPC or ChA. After incubation, cells were stained for H2AX. Fluorescence microscopy images (Zeiss Axio Imager Z2 microscope). Magnification: 63x; scale bar: 20 μm . Etoposide (ETP) for 16h prior to staining at 100 μM (inset of POPC) was used as control for H2AX staining. VSMCs were incubated during 6, 12, 24, 48 and 72h with POPC or ChA, and then mRNA was extracted and analysed for the expression of *Il-1 β* **(H)**, *Il-6* **(I)**, and *Tnf* **(J)**, by RT-qPCR. Data were normalized to the endogenous *Gapdh* and *Pgk1* genes and then normalized to POPC (dashed line). Data represent the mean \pm SD of 3 independent experiments. Statistical significance was assessed by unpaired t-test: *, $p < 0.05$; ns, non-significant. **(K)** Quantification of IL-6 levels in the supernatant of VSMCs treated for 72h with POPC and ChA. Data represent the mean \pm SD of 3 independent experiments, normalized to protein levels. Statistical significance was assessed by unpaired t-test: ns, non-significant.

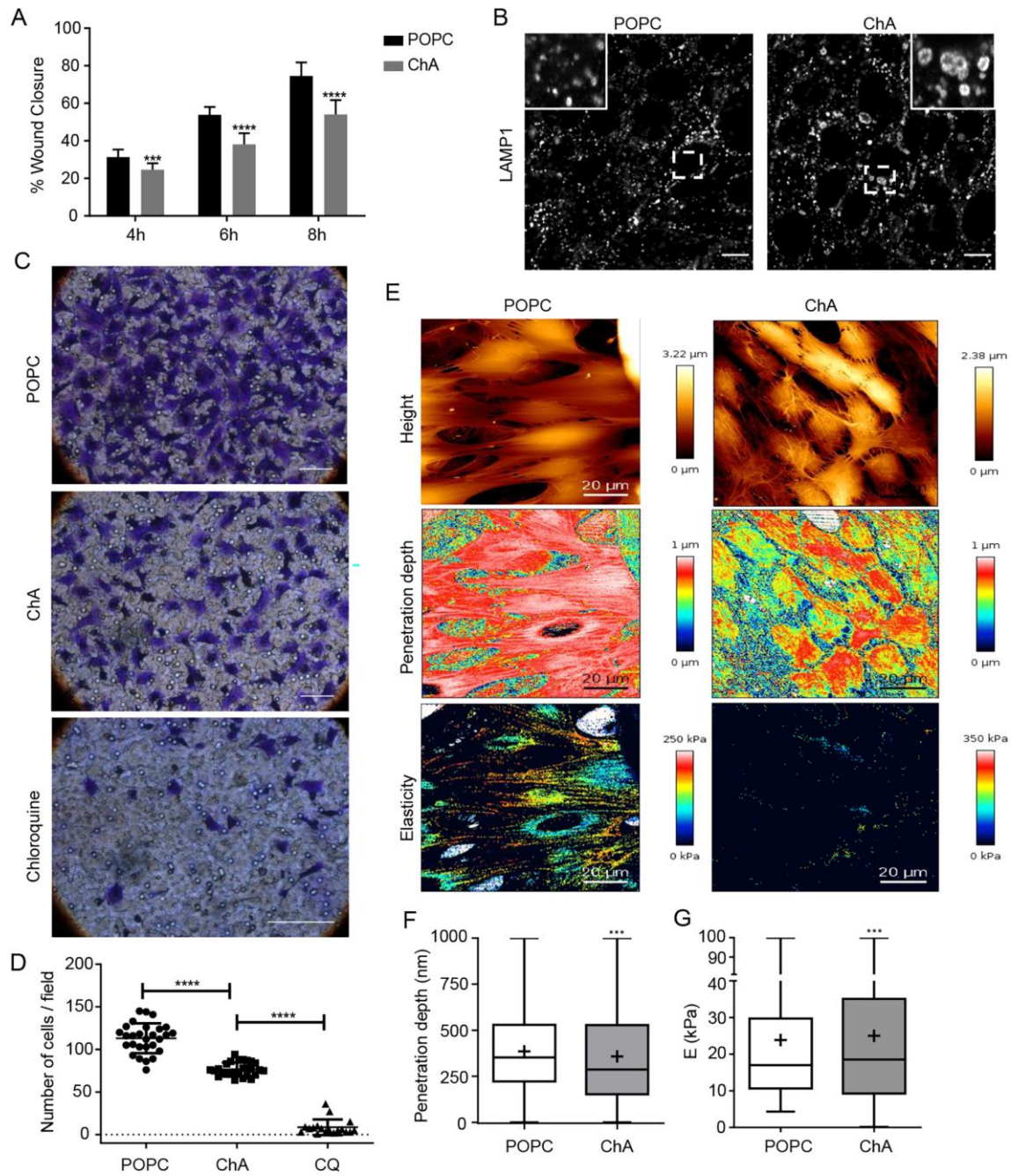


Figure 8: ChA inhibits migration and alters the membrane properties of VSMCs. (A) Percentage of wound closure in VSMCs after 4, 6 and 8h of treatment with POPC and ChA. Data represent the mean \pm SD of 3 independent experiments. Statistical significance was assessed by two-way ANOVA: ***, $p < 0.001$; ****, $p < 0.0001$. (B) After 8h of POPC and ChA treatment, VSMCs were stained with anti-LAMP1 antibody. Insets represent zooms of the regions outlined by the dashed rectangles. Confocal single-slice images magnification: 63x; scale bar: 10 μm . (C) VSMCs were added to the upper chamber of 8-mm-

pore membranes after 72h treatment and allowed to migrate for 2h. Representative fields of crystal violet-stained cells that migrated to the lower surface of the membranes are shown: POPC, ChA and chloroquine (CQ). Magnification: 40x; scale bar: 200 μm . **(D)** Quantification of the number of cells per field that migrated in **(C)**. Data represent the mean \pm SD of 3 independent experiments. Statistical significance was assessed by one-way ANOVA: ****, $p < 0.0001$. **(E)** AFM images of VSMCs treated with POPC and ChA for 72h: QI height (upper panel), elasticity (middle panel) and penetration depth (lower panel). Scale bar: 20 μm . **(F)** Quantification of AFM tip penetration depth onto VSMCs treated with POPC and ChA for 72h, for an applied force of 650 pN. The “+” symbol indicates the average value of penetration depth for each group of 3 independent experiments. Statistical significance was assessed by t-test: ***, $p < 0.001$. **(G)** Quantification of Young’s modulus of VSMCs treated with POPC and ChA for 72h. The “+” symbol indicates the average value of Young’s modulus for each group of 3 independent experiments. Statistical significance was assessed by t-test: ***, $p < 0.001$.

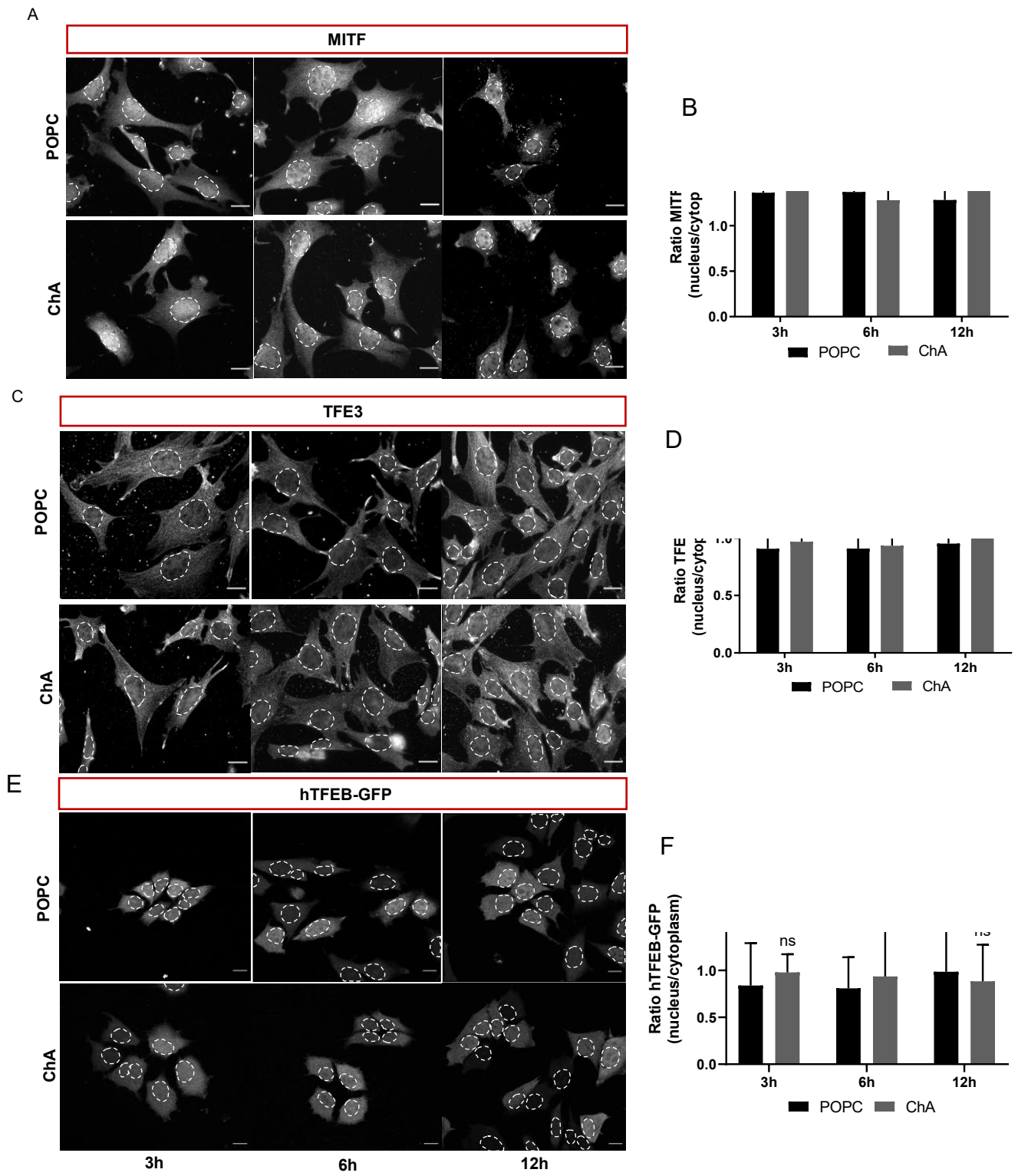


Fig. S1. ChA does not lead to the nuclear translocation of MITF/TFE transcription factors in early time-points. VSMCs were incubated for 3 h (left panel), 6 h (middle panel) and 12 h (right panel) with POPC (upper panel) or ChA (lower panel). After incubation, the cells immunostained with antibodies against MITF **(A)** and TFE3 **(C)**. Fluorescence microscopy images (Zeiss Axio Imager Z2microscope); Magnification: 63x and Scale bar: 20 μ m. TFEB was visualized via the GFP protein fused at the C-terminus of hTFEB **(E)**. Confocal microscopy pictures of hTFEB-GFP (Zeiss LSM980). Magnification: 63x; scale bar: 20 μ m. Nucleus delimited by dashed lines. **(B)**, **(D)** and **(F)** represent the ratio of mean intensity of MITF, TFE3 and hTFEB fluorescence, respectively, of the nucleus with cytoplasm at 3 h, 6 h, 12 h in cells treated with POPC and ChA. Data represent the mean \pm SD of 3 independent experiments. Statistical significance was assessed by 2way ANOVA: ns- non-significant.

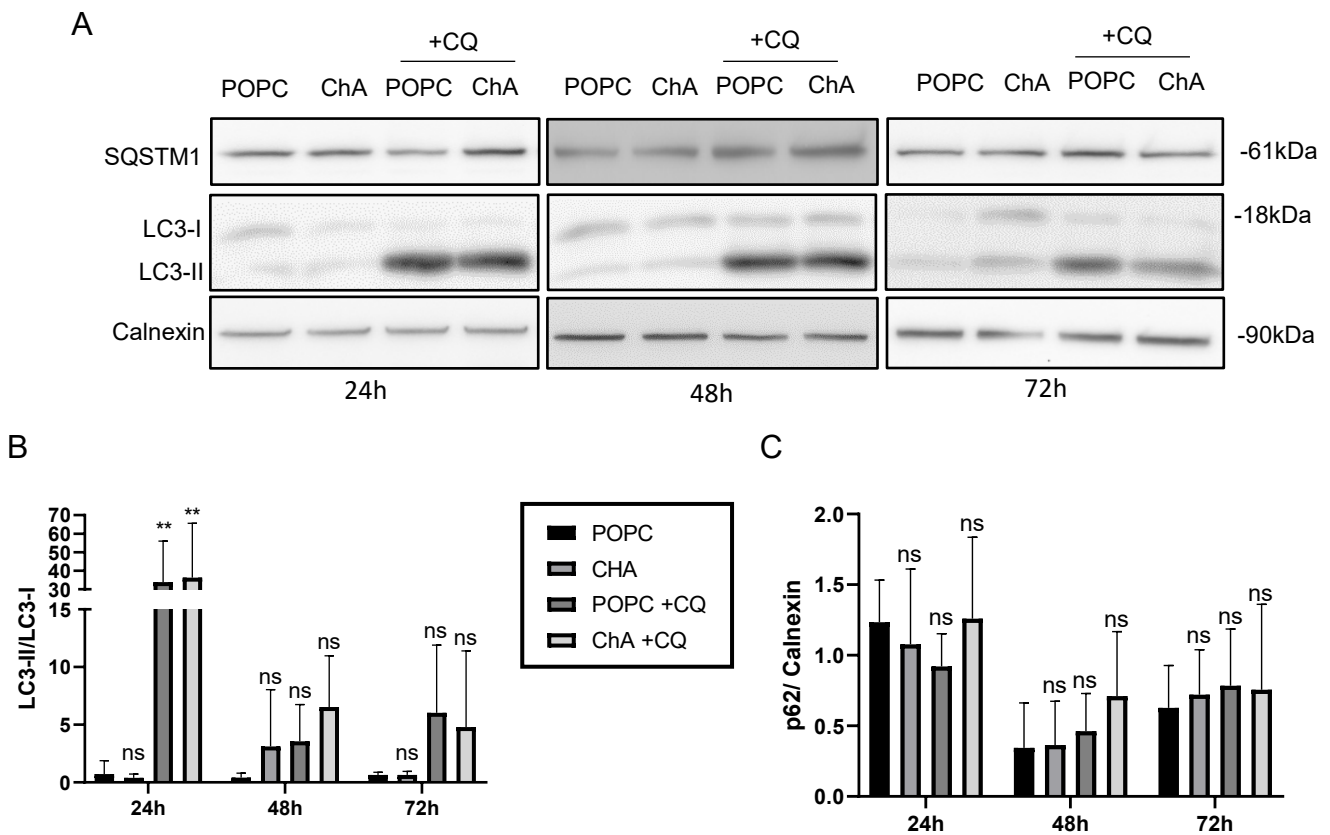


Fig. S2. ChA does not stimulate autophagy in VSMCs. (A) Western blot showing SQSTM1 and LC3 in cells treated with POPC, ChA, and POPC or ChA plus 4 h of chloroquine (CQ) at 24, 48 and 72 h. Calnexin was used as a loading control. **(B)** LC3-II/LC3-I ratio and **(C)** SQSTM1/calnexin ratio of bands obtained in **(A)**. Data represent the mean \pm SD of 3 independent experiments. Statistical significance was assessed by unpaired t-test: *, $p < 0.05$; **, $p < 0.01$; ***, $p < 0.001$; ns, non-significant.

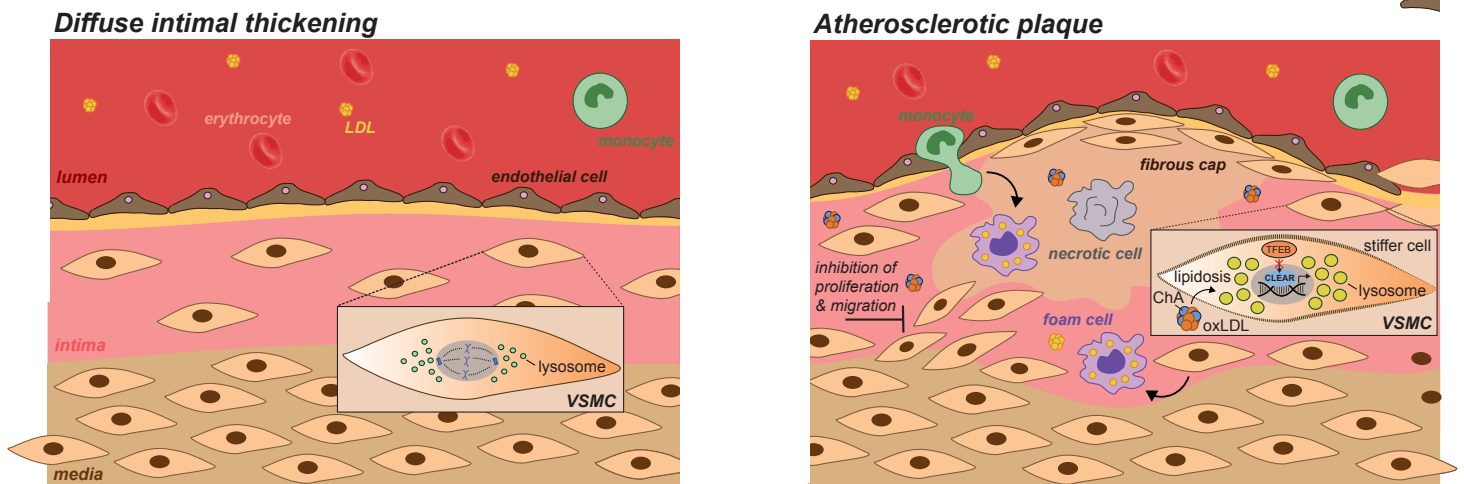


Fig. S3. Model of ChA-induced proatherogenic changes in VSMC homeostasis. Left image: Atherosclerosis-prone artery, in humans VSMCs form a thick layer in the intima known as diffuse intimal thickening (DIT). Right image: During atherosclerotic plaque formation, VSMCs in the intima become foam cells. Medial VSMCs proliferate and migrate into the intima to form a protective fibrous cap, which, in certain conditions, prevents plaque rupture. The uncontrolled uptake of ChA-containing oxLDL by VSMCs (along with macrophages) triggers a change from a contractile to a synthetic phenotype. VSMCs contribute to half of the foam cell population formed through this pathogenic process. In time, foam cells can die by necrosis, releasing their content and aggravating the inflammatory cascade. Exposure to ChA alone can mimic some of these alterations in VSMCs, namely the increase in cell stiffness, inhibition of proliferation and migration, and accumulation of neutral lipids in enlarged (dysfunctional) lysosomes. Changes in lysosome homeostasis are likely the consequence of ChA-induced retention of the TFEB transcription factor in the cytosol, which hinders nuclear transcription of lysosome and autophagy-related genes.

Table S1. Primer sequences

Genes	Sequences	
	Forward	Reverse
<i>Atp6v0d2</i>	CAGAGCTGTACTTCAATGTGGAC	AGGTCTCACACTGCACTAGGT
<i>Ctsb</i>	TCCTTGATCCTTCTTTCTTGCC	ACAGTGCCACACAGCTTCTTC
<i>Ctsd</i>	GCTTCCGGTCTTTGACAACCT	CACCAAGCATTAGTTCTCCTCC
<i>gapdh</i>	GGGAAGCCCATCACCATCTTC	AGAGGGGCCATCCACAGTCT
<i>Il-1β</i>	TGCCACCTTTTGACAGTGATGA	GCGAGATTTGAAGCTGGATGC
<i>Il-6</i>	TCCAGTTGCCTTCTTGGGAC	GTACTCCAGAAGACCAGAGG
<i>ki67</i>	AATCCAACCTCAAGTAAACGGGG	TTGGCTTGCTTCCATCCTCA
<i>Lamp1</i>	ACATCAGCCCAAATGACACA	GGCTAGAGCTGGCATTTCATC
<i>Lamp2b</i>	GGTGCTGGTCTTTTCAAGGCTTGATT	ACCACCCAATCTAAGAGCAGGACT
<i>lc3</i>	GACGGCTTCCTGTACATGGTTT	TGGAGTCTTACACAGCCATTGC
<i>lipa</i>	CTAGAATCTGCCAGCAAGCC	AGTATTCACCGAATCCCTCG
<i>mitf</i>	GCAAGAGGGAGTCATGCAGT	AGTTGCTGGCGTAGCAAGAT
<i>mucolipin1</i>	GCGCCTATGACACCATCAA	TATCCTGGCACTGCTCGAT
<i>p62</i>	GTCTTCTGTGCCTGTGCTGGAA	TCTGCTCCACCAGAAGATCCCA
<i>Pgk1</i>	ATGGATGAGGTGGTCAAAGC	CAGTGCTCACATGGCTGACT
<i>tfe3</i>	CCTGAAGGCATCTGTGGATT	TGTAGGTCCAGAAGGGCATC
<i>tfeb</i>	AGGAGCGGCAGAAGAAAGAC	CAGGTCCTTCTGCATCCTCC
<i>tnf</i>	GTCCCCAAAGGGATGAGAAGT	TTTGCTACGACGTGGGCTAC